JOURNAL OF GUIDANCE, CONTROL, AND DYNAMICS
Vol. 31, No. 1, January–February 2008

Visual Tracking of a Maneuvering Target

Vahram Stepanyan* and Naira Hovakimyan†
Virginia Polytechnic Institute and State University, Blacksburg, Virginia 24061

DOI: 10.2514/1.29758

This paper presents an acceleration-command generation and its implementation for an aerial vehicle in the problem of visual target tracking, when the target is free to make any maneuver with arbitrary but otherwise bounded acceleration. The acceleration command is generated by an adaptive disturbance rejection control algorithm that uses only visual information about the target, obtained by a monocular camera mounted on the aerial vehicle. This information consists of the maximal image size in pixels and the pixel coordinates of the image centroid in the image plane. The acceleration command is translated into forward velocity and attitude angle commands, which are afterward used to obtain actual control surface deflections for the aerial vehicle. Simulations of a full nonlinear model verify the theoretical statements.

I. Introduction

IN AN earlier paper [1], we addressed the problem of visual tracking of a maneuvering target under the assumption that the maneuvers made by the target are such that the integral of its velocity change is bounded. Although restrictive, it is straightforward to note that any maneuver by the target over finite time, such as an obstacle or collision avoidance maneuver, satisfies this assumption. In this paper, we extend the approach to the case of a target moving with arbitrary but otherwise bounded acceleration.

Observability is known to be the main issue in the problems of target tracking with passive monocular sensors, which measure only the line-of-sight (LOS) angle [2,3]. To overcome this issue, [4] proposes to use one more angular measurement: namely, the maximum angle subtended by the target in the image plane. However, this angular measurement cannot recover the observability, because the relative range between the two flying objects is related to it through the target's apparent size, which is, in general, unknown to the follower. Stereo vision can be considered for computation of the target's relative position with respect to the follower, however, the accuracy of calculations will be proportional to the separation of the two cameras, which is negligible in the case of small unmanned aerial vehicles (UAVs). In addition, for small UAVs with two cameras, the images seen by different cameras need to be matched.

Letting the target's apparent size be an unknown constant, the relative dynamics can be written in scaled coordinates that can be computed from visual measurements [1]. This transformation leads to reference commands dependent upon this unknown parameter, which consequently imply that the tracking problem cannot be solved without parameter convergence. The latter can be achieved using an intelligent excitation signal [5], which relates the excitation amplitude to the tracking error, guaranteeing simultaneous convergence for both.

One of the other challenges in the target tracking problem is the compensation for the unknown target's dynamics. The existing results refer to targets moving with constant velocity or model the target's acceleration as a zero-mean Gaussian white process [6–11]. Because the state-space representation for the system is nonlinear either in the states (spherical coordinate system [2,12,13]) or in the measurement equation (Cartesian coordinate system [10,14]), the extended Kalman filter (EKF) or its modifications have been used for extracting necessary information about the target's dynamics and position. However, the convergence properties of the EKF have been proven for a very limited class of systems [15]. In addition, we note that the relative range cannot be recovered from the bearing-only measurements, unless a special type of own-ship maneuver is performed in conjunction with a proper estimation algorithm (see, for example, [16] and citations therein). The adaptive output feedback approach from [17] addresses the tracking problem of a maneuvering target under a certain set of assumptions about the target dynamics.

The results in [1] are derived under the assumption that the target makes only finite maneuvers. We cast the problem into an adaptive disturbance rejection framework for a multi-input/multi-output linear system with unknown high-frequency gain and bounded time-varying disturbances, which have bounded derivatives and are square integrable. The guidance law leads to asymptotic tracking of the reference commands, which depend upon the estimates of the unknown parameters. The latter are updated online and shown to converge to the true values in the presence of intelligent excitation. However, this approach has several limitations: It is applicable only to a limited class of the target maneuvers; the target's apparent size in general cannot be a constant; and the visual information may not be available continuously (that is, the target can be lost from the field of view or whited out).

While the last two limitations are still a subject of ongoing research, we presently remove the first limitation by extending the approach from [1] to allow for arbitrary motion of the target, requiring only boundedness of its acceleration. We retain the main mathematical formulations; however, this extension leads to a higher-order problem formulation that involves relative position, velocity, and acceleration of two flying vehicles. Although the range-estimation scheme is not changed, the guidance law in this paper is an inertial acceleration command, the derivation of which requires an output feedback approach. We reduce the system's relative degree by means of the input-filtered transformation [18] that allows for design of an adaptive observer similar to the one in [19]. The guidance law is derived using adaptive backstepping [20] with adaptive bounding [21]. The derived acceleration command is discontinuous and guarantees asymptotic tracking of the estimated reference commands, simultaneously rejecting the time-varying bounded disturbances. For implementation purposes, the discontinuous acceleration command is approximated by a smooth command that guarantees bounded tracking with an adjustable ultimate bound.

For the inner-loop control design, we translate the guidance law into forward velocity and attitude angle commands. The actual control surface deflections are designed for a full nonlinear aircraft

Presented as Paper 6717 at the AIAA Guidance, Navigation, and Control Conference and Exhibit, Keystone, CO, 21–24 August 2006; received 14 January 2007; revision received 27 July 2007; accepted for publication 30 July 2007.

*Postdoctoral Associate, Department of Mechanical Engineering. Member AIAA.

†Professor, Department of Aerospace and Ocean Engineering. Senior Member AIAA.

model using adaptive block backstepping [20]. Radial basis function (RBF) neural networks are used for approximation of the modeling uncertainties. We note that the inner-loop design is not the objective of this paper and is pursued only for the sake of completeness; namely, to show that the formulated vision-based guidance command can be implemented in at least one way. Magnitude and rate saturation of actual control signals can be addressed following any conventional methods [22].

The rest of the paper is organized as follows. First, we give the problem formulation and derive the state-space representation. The adaptive disturbance rejection guidance law is presented next. The aerial vehicle's desired motion is formulated, and adaptive block backstepping is presented for derivation of the actual control surface deflections. Throughout the manuscript, bold symbols are used for vectors, capital letters for matrices, small letters for scalars, $\|\cdot\|$ denotes the Euclidean norm, and $\|\cdot\|_F$ denotes the Frobenius norm.

II. Problem Formulation

A. Relative Motion

Equations of motion of a flying target can be given by

$$\ddot{\boldsymbol{R}}_T(t) = \boldsymbol{a}_T(t), \qquad \boldsymbol{R}_T(0) = \boldsymbol{R}_{T_0}, \qquad \dot{\boldsymbol{R}}_T(0) = \boldsymbol{V}_{T_0} \tag{1}$$

where $\boldsymbol{R}_T(t) = [x_T(t) \quad y_T(t) \quad z_T(t)]^\top$ and $\boldsymbol{a}_T(t) = [a_{T_x}(t) \quad a_{T_y}(t) \quad a_{T_z}(t)]^\top$ are, respectively, the position vector and the acceleration of the target's center of gravity in the inertial frame $F_E = (x_E, y_E, z_E)$. The follower's dynamics are given by

$$\ddot{\boldsymbol{R}}_F(t) = \boldsymbol{a}_F(t), \qquad \boldsymbol{R}_F(0) = \boldsymbol{R}_{F_0}, \qquad \dot{\boldsymbol{R}}_F(0) = \boldsymbol{V}_{F_0} \tag{2}$$

where $\boldsymbol{R}_F(t) = [x_F(t) \quad y_F(t) \quad z_F(t)]^\top$ and $\boldsymbol{a}_F(t) = [a_{F_x}(t) \quad a_{F_y}(t) \quad a_{F_z}(t)]^\top$ are, respectively, the follower's position vector and acceleration in the same inertial frame.

We assume that the follower can measure its own states and can get visual information about the target via a camera that is fixed on the follower with its optical axis parallel to the follower's longitudinal x_B axis of the body frame $F_B = (x_B, y_B, z_B)$ and its optical center fixed at the center of gravity of the follower. Then the body frame can be chosen coincident with the camera frame (see Fig. 1a). It is assumed that the image-processing algorithm associated with the visual sensor provides three measurements in real time. These are the pixel coordinates of the image centroid (y_I, z_I) in the image plane I and the image length b_I in pixels (see Fig. 1b). Assuming that the camera focal length l is known, the bearing angle λ and the elevation angle ϑ can be expressed via the measured variables through the geometric relationships

$$\tan\lambda = \frac{y_I}{l}, \qquad \tan\vartheta = \frac{z_I}{\sqrt{l^2 + y_I^2}} \tag{3}$$

The target's relative position with respect to the follower is given by the inertial vector (see Fig. 1a)

$$\boldsymbol{R} = \boldsymbol{R}_T - \boldsymbol{R}_F \tag{4}$$

Hence, the relative dynamics in the inertial frame are given by the equations

$$\ddot{\boldsymbol{R}}(t) = \boldsymbol{a}_T(t) - \boldsymbol{a}_F(t), \qquad \boldsymbol{R}(0) = \boldsymbol{R}_0, \qquad \dot{\boldsymbol{R}}(0) = \boldsymbol{V}_0 \tag{5}$$

where the initial conditions are given by $\boldsymbol{R}_0 = \boldsymbol{R}_{T_0} - \boldsymbol{R}_{F_0}$ and $\boldsymbol{V}_0 = \boldsymbol{V}_{T_0} - \boldsymbol{V}_{F_0}$.

B. Measurement Transformation

We first observe that $R(t) = \|\boldsymbol{R}(t)\|$ can be expressed as

$$R = \frac{b}{b_I}\sqrt{l^2 + y_I^2 + z_I^2} \triangleq b a_I \tag{6}$$

where $b > 0$ is the maximum visible size of the target, which is assumed to be constant. Therefore, the relative position can be expressed in the follower's body frame as follows:

$$\boldsymbol{R}^B = R\boldsymbol{T}_{IB} = b a_I \boldsymbol{T}_{IB} \tag{7}$$

where

$$\boldsymbol{T}_{IB} = \begin{bmatrix} \cos\vartheta\cos\lambda \\ \cos\vartheta\sin\lambda \\ -\sin\vartheta \end{bmatrix} \tag{8}$$

Using the coordinate transformation matrix $L_{B/E}$ from the inertial frame F_E to the follower's body frame F_B given by

$$L_{B/E} = \begin{bmatrix} \cos\theta\cos\psi & \cos\theta\sin\psi & -\sin\theta \\ \sin\phi\sin\theta\cos\psi - \cos\phi\sin\psi & \sin\phi\sin\theta\sin\psi + \cos\phi\cos\psi & \sin\phi\cos\theta \\ \cos\phi\sin\theta\cos\psi + \sin\phi\sin\psi & \cos\phi\sin\theta\sin\psi - \sin\phi\cos\psi & \cos\phi\cos\theta \end{bmatrix}$$

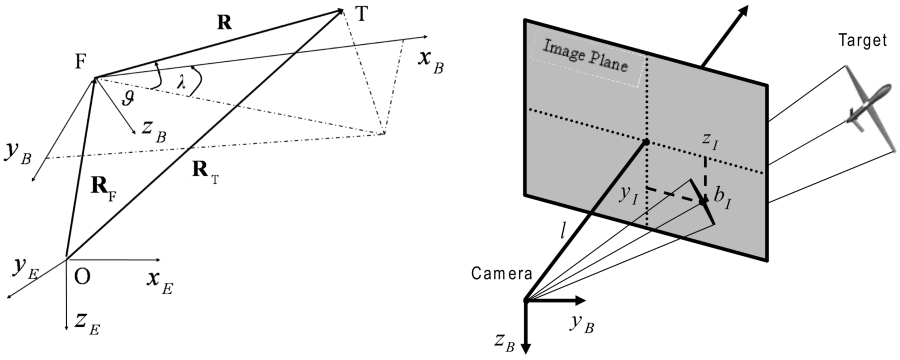

a) Coordinate frames and angles definition **b) Camera frame and measurements**

Fig. 1 Coordinate illustrations.

where ϕ, θ, and ψ are the Euler angles associated with the frame F_B (see [23] p. 313), the inertial relative position vector $\boldsymbol{R}$ can be written as

$$\boldsymbol{R} = L_{B/E}^{\top}\boldsymbol{R}^{B} = ba_I L_{B/E}^{\top}\boldsymbol{T}_{IB} \tag{9}$$

In this form, the relative position is computable up to the unknown scaling factor b. Therefore, we introduce the scaled relative-position vector $\boldsymbol{r}(t) = \boldsymbol{R}(t)/b$, the dynamics of which are written as

$$\ddot{\boldsymbol{r}}(t) = \frac{\boldsymbol{a}_T(t) - \boldsymbol{a}_F(t)}{b}, \qquad \boldsymbol{r}(0) = \boldsymbol{r}_0, \qquad \dot{\boldsymbol{r}}(0) = \boldsymbol{v}_0 \tag{10}$$

where $\boldsymbol{r}_0 = \boldsymbol{R}_0/b$ and $\boldsymbol{v}_0 = \boldsymbol{V}_0/b$. The vector $\boldsymbol{r}$ is related to the visual measurements via the algebraic equation

$$\boldsymbol{r} = a_I L_{B/E}^{\top}\boldsymbol{T}_{IB} \tag{11}$$

and hence is available for feedback; however, $\dot{\boldsymbol{r}}(t)$ is not available.

Thus, the problem is reduced to designing an adaptive output feedback disturbance rejection controller for the matrix second-order system in Eq. (10) that can guarantee desired relative separation from the target. We note that the control input in Eq. (10) is $\boldsymbol{a}_F(t)$, whereas the desired relative separation $\boldsymbol{r}_c(t) = \boldsymbol{R}_c(t)/b$ depends on the unknown constant b.

Remark 1. We note that the conventional guidance laws require the knowledge of one or more of the following quantities: relative range, line-of-sight angle rate, time to go, target's velocity, and target's acceleration bound [11,24–27]. None of these quantities can be obtained from the single camera, which is assumed to be the only sensor giving information about the target's relative position and dynamics.

III. Acceleration Command for Visual Guidance

The control design problem formulated in the previous section implies defining an adaptive output feedback disturbance rejection controller for the linear system in Eq. (10) that has a vector relative degree of $[2 \quad 2 \quad 2]$. To proceed with the control architecture for the preceding formulated problem, we follow the methodology in [18] and introduce the so-called input-filtered state transformation that keeps the output unchanged while transforming the system into one with relative degree 1 in each control channel. The only difference from [18] is that we also need to filter the disturbance along with the input to achieve the desired property. Because the disturbance is unknown, this step seems to be unimplementable, but as we show later, this step is only needed for analysis purposes.

The relative dynamics in Eq. (10) can be written in the matrix form as follows:

$$\begin{gathered}\dot{\boldsymbol{x}}(t) = A\boldsymbol{x}(t) + \frac{1}{b}B[\boldsymbol{a}_T(t) - \boldsymbol{a}_F(t)], \qquad \boldsymbol{x}(0) = \boldsymbol{x}_0 \\ \boldsymbol{y}(t) = C\boldsymbol{x}(t)\end{gathered} \tag{12}$$

where $\boldsymbol{x}(t) = [\,r_x(t) \quad \dot{r}_x(t) \quad r_y(t) \quad \dot{r}_y(t) \quad r_z(t) \quad \dot{r}_z(t)\,]^{\top}$ is the system's state, b is the unknown parameter, $\boldsymbol{a}_F(t)$ is the follower's control input, $\boldsymbol{a}_T(t)$ is the bounded disturbance, $\boldsymbol{y}(t) = [\,r_x(t) \quad r_y(t) \quad r_z(t)\,]^{\top}$ is the regulated output, which is available for feedback, and

$$A = \begin{bmatrix} \mathcal{A} & 0 & 0 \\ 0 & \mathcal{A} & 0 \\ 0 & 0 & \mathcal{A} \end{bmatrix}, \qquad B = \begin{bmatrix} \mathcal{B} & 0 & 0 \\ 0 & \mathcal{B} & 0 \\ 0 & 0 & \mathcal{B} \end{bmatrix}$$

$$C = \begin{bmatrix} \mathcal{C} & 0 & 0 \\ 0 & \mathcal{C} & 0 \\ 0 & 0 & \mathcal{C} \end{bmatrix}$$

where the matrices $\mathcal{A}$, $\mathcal{B}$, and $\mathcal{C}$ are in controllable-observable-canonical forms:

$$\mathcal{A} = \begin{bmatrix} 0 & 1 \\ 0 & 0 \end{bmatrix}, \qquad \mathcal{B} = \begin{bmatrix} 0 \\ 1 \end{bmatrix}, \qquad \mathcal{C} = [\,1 \quad 0\,]$$

The reference command for the system in Eq. (12) is given by

$$\boldsymbol{y}_c(t) = \frac{1}{b}\boldsymbol{R}_c(t)$$

A. Input-Filtered Transformation

Consider the following transformation of coordinates for the system in Eq. (12):

$$\boldsymbol{z}(t) = \boldsymbol{x}(t) - \frac{1}{b}B[\boldsymbol{w}(t) + \boldsymbol{d}(t)] \tag{13}$$

in which $\boldsymbol{w}(t)$ and $\boldsymbol{d}(t)$ are generated via the following stable filters:

$$\begin{aligned}\dot{\boldsymbol{w}}(t) &= \Lambda\boldsymbol{w}(t) - \boldsymbol{a}_F(t), \qquad \boldsymbol{w}(0) = \boldsymbol{0} \\ \dot{\boldsymbol{d}}(t) &= \Lambda\boldsymbol{d}(t) + \boldsymbol{a}_T(t), \qquad \boldsymbol{d}(0) = \boldsymbol{0}\end{aligned} \tag{14}$$

where

$$\Lambda = \begin{bmatrix} -\lambda_1 & 0 & 0 \\ 0 & -\lambda_2 & 0 \\ 0 & 0 & -\lambda_3 \end{bmatrix}$$

and $\lambda_1 > 0$, $\lambda_2 > 0$, and $\lambda_3 > 0$ are design constants. Here, we note that the bounded disturbance $\boldsymbol{a}_T(t)$ in the second filter in Eq. (14) will generate a bounded output $\boldsymbol{d}(t)$, because the matrix Λ is Hurwitz. Thus, there exist unknown constants $d_{Ti} > 0$ ($i = 1, 2, 3$) such that $|d_i(t)| \le d_{Ti}$ for all $t \ge 0$. In the synthesis approach later, we will use the adaptive bounding technique from [21] to adapt to these unknown constants d_{Ti}.

Differentiating both sides of Eq. (13) and taking into account Eqs. (12) and (14), we obtain the following equation:

$$\dot{\boldsymbol{z}}(t) = A\boldsymbol{z}(t) + \frac{1}{b}[AB + B\Lambda][\boldsymbol{w}(t) + \boldsymbol{d}(t)] \tag{15}$$

It is straightforward to verify that the pair $(A, \bar{B})$ is controllable, where $\bar{B} = AB + B\Lambda = \mathrm{diag}(\mathcal{B}_1, \mathcal{B}_2, \mathcal{B}_3)$ and $\mathcal{B}_i = [1 \quad \lambda_i]^{\top}$, where $i = 1, 2, 3$. Because $CB = 0$, the output in Eq. (12) can be equivalently written as $\boldsymbol{y}(t) = C\boldsymbol{z}(t)$. Thus, the system in Eq. (12) is transformed into one with the transmission zeros in the left half-plane and with the well-defined vector relative degree of $[1 \quad 1 \quad 1]$ from the input $\boldsymbol{w}(t) + \boldsymbol{d}(t)$ to the output $\boldsymbol{y}(t)$:

$$\begin{gathered}\dot{\boldsymbol{z}}(t) = A\boldsymbol{z}(t) + \frac{1}{b}\bar{B}[\boldsymbol{w}(t) + \boldsymbol{d}(t)] \\ \boldsymbol{y}(t) = C\boldsymbol{z}(t)\end{gathered} \tag{16}$$

Here, we note that by means of the transformations in Eqs. (13) and (14), the control objective can be realized in two steps. First, we need to design a control input $\boldsymbol{w}_c(t)$ for the system in Eq. (16) in the presence of the unknown parameter $1/b$ and bounded disturbance $\boldsymbol{d}(t)$ to adaptively track the reference command $\boldsymbol{y}_c(t)$. Next, we design a control input $\boldsymbol{a}_F(t)$ for the system in Eq. (14) to track the reference command $\boldsymbol{w}_c(t)$ using conventional block backstepping [20].

B. Reference Model

The controller $\boldsymbol{w}(t)$ for the system in Eq. (16) is designed by augmenting the conventional model-reference adaptive control scheme with a robustifying term to compensate for the unknown disturbance $\boldsymbol{d}(t)$. Toward this end, we first need to design a reference model:

$$\begin{gathered}\dot{\boldsymbol{z}}_m(t) = A_m\boldsymbol{z}(t) + B_m\boldsymbol{y}_c(t) \\ \boldsymbol{y}_m(t) = C\boldsymbol{z}_m(t)\end{gathered} \tag{17}$$

Because the matrices A, $\bar{B}$, and C are block diagonal, it is natural to select a block diagonal matrix,

$$K = \begin{bmatrix} \mathcal{K}_1 & 0 & 0 \\ 0 & \mathcal{K}_2 & 0 \\ 0 & 0 & \mathcal{K}_3 \end{bmatrix}$$

such that

$$A_m = A - \bar{B}K = \begin{bmatrix} \mathcal{A}_{m1} & 0 & 0 \\ 0 & \mathcal{A}_{m2} & 0 \\ 0 & 0 & \mathcal{A}_{m3} \end{bmatrix}$$

$$B_m = \bar{B}KC^\top = \begin{bmatrix} \mathcal{B}_{m1} & 0 & 0 \\ 0 & \mathcal{B}_{m2} & 0 \\ 0 & 0 & \mathcal{B}_{m3} \end{bmatrix}$$

where $\mathcal{A}_{mi} = \mathcal{A} - \mathcal{B}_i\mathcal{K}_i$ $(i = 1, 2, 3)$ and $\mathcal{B}_{mi} = \mathcal{B}_i\mathcal{K}_i\mathcal{C}^\top$ $(i = 1, 2, 3)$. Here, $\mathcal{K}_i = [\, k_{i1} \quad k_{i2} \,]$ $(i = 1, 2, 3)$. It is straightforward to verify that if $k_{i1} > 0$, $k_{i1} + \lambda_i k_{i2} > 0$ $(i = 1, 2, 3)$, then A_m is Hurwitz, and the transfer function from the input $y_{ci}(t)$ to the output $y_{mi}(t)$ is

$$G_i(s) = k_{i1}\frac{s + \lambda_i}{s^2 + (k_{i1} + \lambda_i k_{i2})s + \lambda_i k_{i1}} \tag{18}$$

It follows that $G_i(s) \to 1$ as $s \to 0$; that is, $\boldsymbol{y}_m(t) \to \boldsymbol{y}_c$ as $t \to \infty$ for a constant $\boldsymbol{y}_c$ command. It can be shown by straightforward computation that if k_{i1} and k_{i2} satisfy $k_{i1} + \lambda_i k_{i2} \geq \lambda_i$, then $G_i(s)$ is strictly positive real (SPR). Then following the Kalman-Yakubovich-Popov Lemma [28], there exists $P_1 = P_1^\top > 0$ and $Q_1 > 0$ such that

$$A_m^\top P_1 + P_1 A_m = -Q_1, \qquad P_1\bar{B} = C^\top \tag{19}$$

C. Stabilizing Virtual Controller Design

First, we introduce the stabilizing virtual controller for the dynamics in Eq. (16) that depend upon the unknown parameters. Consider the following structure:

$$\boldsymbol{w}_c(t) = \hat{b}(t)\boldsymbol{h}(t) - S(\cdot)\hat{\boldsymbol{d}}(t), \qquad \boldsymbol{h}(t) = -K\hat{\boldsymbol{z}}(t) + KC^\top \boldsymbol{y}_c(t) \tag{20}$$

where $\hat{\boldsymbol{z}}(t)$ is the estimate of the state $\boldsymbol{z}(t)$, governed by the following dynamics:

$$\begin{gathered} \dot{\hat{\boldsymbol{z}}}(t) = A_m\hat{\boldsymbol{z}}(t) + B_m\boldsymbol{y}_c(t) + L[\boldsymbol{y}(t) - \hat{\boldsymbol{y}}(t)] \\ \hat{\boldsymbol{y}}(t) = C\hat{\boldsymbol{z}}(t) \end{gathered} \tag{21}$$

where $\hat{b}(t)$ is the estimate of the unknown parameter b, $\hat{\boldsymbol{d}}(t)$ is the estimate of the unknown bound $\boldsymbol{d}_T$, and $S(\cdot)$ is a robustifying matrix function to be defined shortly. At first we need to show that $\boldsymbol{w}_c(t)$ in Eq. (20) stabilizes the $\boldsymbol{z}$ dynamics in Eq. (16) in the absence of filters from Eq. (14). Toward that end, we directly substitute it into Eq. (16):

$$\begin{aligned} \dot{\boldsymbol{z}}(t) &= A\boldsymbol{z}(t) + \frac{1}{b}\bar{B}\{[b + \tilde{b}(t)][-K\hat{\boldsymbol{z}}(t) + KC^\top \boldsymbol{y}_c(t)] \\ &\quad + \boldsymbol{d}(t) - S(\cdot)\hat{\boldsymbol{d}}(t)\} = A_m\boldsymbol{z}(t) + B_m\boldsymbol{y}_c(t) + \bar{B}K\tilde{\boldsymbol{z}}(t) \\ &\quad + \frac{1}{b}\bar{B}[\tilde{b}(t)\boldsymbol{h}(t) + \boldsymbol{d}(t) - S(\cdot)\hat{\boldsymbol{d}}(t)] \end{aligned} \tag{22}$$

where $\tilde{b}(t) = \hat{b}(t) - b$ is the parameter estimation error and $\tilde{\boldsymbol{z}}(t) = \boldsymbol{z}(t) - \hat{\boldsymbol{z}}(t)$ is the state estimation error, the dynamics of which can be derived straightforwardly:

$$\begin{gathered} \dot{\tilde{\boldsymbol{z}}}(t) = (A - LC)\tilde{\boldsymbol{z}}(t) + \frac{1}{b}\bar{B}[\tilde{b}(t)\boldsymbol{h}(t) + \boldsymbol{d}(t) - S(\cdot)\hat{\boldsymbol{d}}(t)] \\ \tilde{\boldsymbol{y}}(t) = C\tilde{\boldsymbol{z}}(t) \end{gathered} \tag{23}$$

The gain matrix L is chosen to render $A_o = A - LC$ Hurwitz and to ensure that the transfer matrix $G_o(s) = C(sI - A_o)^{-1}\bar{B}$ is SPR. Naturally, it can be chosen in block diagonal form:

$$L = \begin{bmatrix} L_1 & 0 & 0 \\ 0 & L_2 & 0 \\ 0 & 0 & L_3 \end{bmatrix}, \qquad L_i = \begin{bmatrix} l_{i1} \\ l_{i2} \end{bmatrix}$$

where $i = 1, 2, 3$. Then

$$A_o = \begin{bmatrix} \mathcal{A}_{o1} & 0 & 0 \\ 0 & \mathcal{A}_{o2} & 0 \\ 0 & 0 & \mathcal{A}_{o3} \end{bmatrix}, \qquad \mathcal{A}_{oi} = \mathcal{A}_i - L_i\mathcal{C}$$

where $i = 1, 2, 3$, and

$$G_o(s) = \begin{bmatrix} G_{o1}(s) & 0 & 0 \\ 0 & G_{o2}(s) & 0 \\ 0 & 0 & G_{o3}(s) \end{bmatrix}$$

$$G_{oi}(s) = \frac{s + \lambda_i}{s^2 + l_{i1}s + l_{i2}}$$

where $i = 1, 2, 3$. Hence, if A_{o1}, A_{o2}, and A_{o3} are Hurwitz and $G_{o1}(s)$, $G_{o2}(s)$, and $G_{o3}(s)$ are SPR, then A_o is Hurwitz and $G_o(s)$ is SPR. This can be ensured by choosing $l_{i1} \geq \lambda_i$ and $l_{i2} > 0$. Then following the Kalman-Yakubovich-Popov Lemma, there exist $P_2 = P_2^\top > 0$ and $Q_2 = Q_2^\top > 0$ such that

$$A_o^\top P_2 + P_2 A_o = -Q_2, \qquad P_2\bar{B} = C^\top \tag{24}$$

Denoting the tracking error by $\boldsymbol{e}(t) = \boldsymbol{z}(t) - \boldsymbol{z}_m(t)$, the error dynamics are written as

$$\begin{gathered} \dot{\boldsymbol{e}}(t) = A_m\boldsymbol{e}(t) + \bar{B}K\tilde{\boldsymbol{z}}(t) + \frac{1}{b}\bar{B}[\tilde{b}(t)\boldsymbol{h}(t) + \boldsymbol{d}(t) - S(\cdot)\hat{\boldsymbol{d}}(t)] \\ \boldsymbol{e}_c(t) = C\boldsymbol{e}(t) \end{gathered} \tag{25}$$

Introducing the parameter estimation error $\tilde{\boldsymbol{d}}(t) = \hat{\boldsymbol{d}}(t) - \boldsymbol{d}_T$, we combine both the tracking and the state estimation error dynamics in Eq. (23) and in the following equation:

$$\begin{gathered} \dot{\boldsymbol{\xi}}_a(t) = A_a\boldsymbol{\xi}_a(t) + \frac{1}{b}B_a[\tilde{b}(t)\boldsymbol{h}(t) + \boldsymbol{d}(t) - S(\cdot)\boldsymbol{d}_T - S(\cdot)\tilde{\boldsymbol{d}}(t)] \\ \boldsymbol{y}_a(t) = C_a\boldsymbol{\xi}_a(t) \end{gathered} \tag{26}$$

where

$$\boldsymbol{\xi}_a = \begin{bmatrix} \boldsymbol{e} \\ \tilde{\boldsymbol{z}} \end{bmatrix}, \qquad \boldsymbol{y}_a = \begin{bmatrix} \boldsymbol{e}_c \\ \tilde{\boldsymbol{y}} \end{bmatrix}, \qquad A_a = \begin{bmatrix} A_m & \bar{B}K \\ 0_{6\times 6} & A_o \end{bmatrix}$$

$$B_a = \begin{bmatrix} \bar{B} \\ \bar{B} \end{bmatrix}, \qquad C_a = [\, C \quad C \,]$$

Now we can define the matrix function $S(\cdot)$ as follows:

$$S(\boldsymbol{y}_a) = \begin{bmatrix} \operatorname{sgn}(y_{a1}) & 0 & 0 \\ 0 & \operatorname{sgn}(y_{a2}) & 0 \\ 0 & 0 & \operatorname{sgn}(y_{a3}) \end{bmatrix} \tag{27}$$

where the function $\operatorname{sgn}(\cdot)$ is defined as

$$\operatorname{sgn}(x) = \begin{cases} 1 & x > 0 \\ 0 & x = 0 \\ -1 & x < 0 \end{cases} \tag{28}$$

From the relationships in Eqs. (19) and (24), it follows that

$$A_a^\top P_a + P_a A_a = -Q_a, \qquad P_a B_a = C_a^\top \tag{29}$$

where

$$P_a = \begin{bmatrix} P_1 & 0_{6\times 6} \\ 0_{6\times 6} & P_2 \end{bmatrix}, \qquad Q_a = \begin{bmatrix} Q_1 & 0_{6\times 6} \\ 0_{6\times 6} & Q_2 \end{bmatrix}$$

Notice that the function $S(\boldsymbol{y}_a)$ is discontinuous. Consequently, the estimation and tracking error dynamics have discontinuous

right-hand sides. Results on existence and uniqueness of the solution for such systems and the application of Lyapunov stability theory are developed in [29]. In [19], we have a detailed overview of their applicability to the specific design problem discussed here.

To complete the controller design, we need the adaptive laws for the online update of parameter estimates $\hat{b}(t)$ and $\hat{\boldsymbol{d}}(t)$; these are given as follows:

$$\dot{\hat{\boldsymbol{d}}}(t) = GS(\boldsymbol{y}_a(t))\boldsymbol{y}_a(t), \qquad \hat{\boldsymbol{d}}(0) = \boldsymbol{0} \tag{30}$$

$$\dot{\hat{b}}(t) = \rho \text{Proj}(\hat{b}(t), -\boldsymbol{y}_a^\top(t)\boldsymbol{h}(t)), \qquad \hat{b}(0) = b_0 > b_{\min} \tag{31}$$

where $\rho > 0$ and $G > 0$ are constant adaptation gains; $b_{\min}$ is a known conservative lower bound for b; and $\text{Proj}(\cdot,\cdot)$ is the projection operator , defined as follows:

$$\text{Proj}\,(p, y) = \begin{cases} y & \text{if } f(p) < 0 \\ y & \text{if } f(p) \geq 0 \quad y\nabla f \leq 0 \\ y[1 - f(p)] & \text{if } f(p) \geq 0 \quad y\nabla f > 0 \end{cases}$$

where the convex function $f(\cdot)$ is defined using the available conservative bounds on the parameter p. Given the conservative bounds $0 < b_{\min} \leq b \leq b_{\max}$ for b, the function f can be chosen as

$$f(\hat{b}) = \epsilon_b^{-1}\left[\left(\hat{b} - \frac{b_{\max} + b_{\min}}{2}\right)^2 - \left(\frac{b_{\max} - b_{\min}}{2}\right)^2\right] \tag{32}$$

where ϵ_b denotes the convergence tolerance of our choice. It can be proved that the adaptive law in Eq. (31) guarantees the following inequalities [30]:

$$\begin{gathered} b_{\min} \leq \hat{b}(t) \leq b_{\max} \\ \tilde{b}(t)[\boldsymbol{y}_a^\top(t)\boldsymbol{h}(t) + \text{Proj}(\hat{b}(t), -\boldsymbol{y}_a^\top(t)\boldsymbol{h}(t))] \leq 0 \end{gathered} \tag{33}$$

The stability of error dynamics is given by the following theorem:

Theorem 1. The robust adaptive virtual controller $\boldsymbol{w}_c(t)$ in Eq. (20), along with the adaptive laws in Eqs. (30) and (31), guarantees uniform global boundedness of all error signals and asymptotic convergence of $\boldsymbol{\xi}_a(t)$ to zero.

Proof. We choose a candidate Lyapunov function dependent on the states in Eqs. (26), (30), and (31):

$$V_1(\boldsymbol{\xi}_a(t), \tilde{b}(t), \tilde{\boldsymbol{d}}(t)) = \boldsymbol{\xi}_a^\top(t)P_a\boldsymbol{\xi}_a(t) + \frac{1}{b}\left[\frac{\tilde{b}^2(t)}{\rho} + \tilde{\boldsymbol{d}}^\top(t)G^{-1}\tilde{\boldsymbol{d}}(t)\right] \tag{34}$$

The derivative of $V_1(t)$ along the trajectories of the systems in Eqs. (25), (30), and (31) has the form

$$\begin{aligned} \dot{V}_1(t) &= \boldsymbol{\xi}_a^\top(t)[A_a^\top P_a + P_a A_a]\boldsymbol{\xi}_a(t) + \frac{2}{b}\left[\frac{\tilde{b}(t)}{\rho}\dot{\tilde{b}}(t)\right. \\ &\quad \left. + \tilde{\boldsymbol{d}}^\top(t)G^{-1}\dot{\tilde{\boldsymbol{d}}}(t)\right] + 2\boldsymbol{\xi}_a^\top(t)P_a\frac{1}{b}B_a[\tilde{b}(t)\boldsymbol{h}(t) + \boldsymbol{d}(t) \\ &\quad - S(\boldsymbol{y}_a(t))\boldsymbol{d}_T - S(\boldsymbol{y}_a(t)]\tilde{\boldsymbol{d}}(t)) = -\boldsymbol{\xi}_a^\top(t)Q_a\boldsymbol{\xi}_a(t) \\ &\quad + \frac{2\tilde{b}(t)}{b}\left(\boldsymbol{y}_a^\top(t)\boldsymbol{h}(t) + \frac{1}{\rho}\dot{\tilde{b}}(t)\right) + \frac{2}{b}\tilde{\boldsymbol{d}}^\top(t)[-S(\boldsymbol{y}_a(t))\boldsymbol{y}_a(t) \\ &\quad + G^{-1}\dot{\tilde{\boldsymbol{d}}}(t)] + \frac{2}{b}\boldsymbol{\xi}_a^\top(t)P_aB_a[\boldsymbol{d}(t) - S(\boldsymbol{y}_a(t))\boldsymbol{d}_T] \end{aligned} \tag{35}$$

We note that $\dot{V}_1(t)$ is discontinuous due to the discontinuity of $S(\boldsymbol{y}_a(t))$ on the switching manifold $\Omega_S = \{\boldsymbol{\xi}_a\colon C_a\boldsymbol{\xi}_a = \boldsymbol{y}_a = 0\}$. Following [31], we need to calculate $\dot{V}_1(t)$ on the switching manifold Ω_S and away from it. However, in both cases, we obtain the same upper bound for $\dot{V}_1(t)$, because

$$\boldsymbol{\xi}_a^\top(t)P_aB_a = \boldsymbol{\xi}_a^\top(t)C_a^\top = \boldsymbol{y}_a^\top(t)$$

and the last term in Eq. (35) can be upper-bounded as follows:

$$\boldsymbol{y}_a^\top[\boldsymbol{d}(t) - S(\boldsymbol{y}_a(t))\boldsymbol{d}_T] = \sum_{i=1}^{3}[y_{ai}(t)d_i(t) - |y_{ai}(t)|d_{Ti}] \leq 0 \tag{36}$$

Upon substitution of the adaptive laws from Eqs. (30) and (31), and using the properties of the projection operator from Eq. (33), we conclude that

$$\dot{V}_1(t) \leq -\boldsymbol{\xi}_a^\top(t)Q_a\boldsymbol{\xi}_a(t) \leq -\lambda_{\min}(Q_a)\|\boldsymbol{\xi}_a(t)\|^2 \tag{37}$$

where $\lambda_{\min}(Q_a)$ denotes the minimum eigenvalue of the matrix Q_a. Because the inequalities in Eqs. (33) and (36) hold for any value of $\boldsymbol{y}_a(t)$, the inequality in Eq. (37) holds globally, implying that the signals $\boldsymbol{\xi}_a(t)$, $\tilde{b}(t)$, and $\tilde{\boldsymbol{d}}(t)$ are globally bounded. It follows that $V_1(t)$ is also bounded. Integration of the inequality in Eq. (37) results in

$$\lim_{t\to\infty}\int_0^t \lambda_{\min}(Q_a)\|\boldsymbol{\xi}_a(\tau)\|^2\,\mathrm{d}\tau \leq \lim_{t\to\infty}[V_1(0) - V_1(t)] < \infty \tag{38}$$

Because $\boldsymbol{y}_c(t)$ is bounded, the reference state $\boldsymbol{z}_m(t)$ is bounded, which implies boundedness of the state $\boldsymbol{z}(t)$ and, consequently, the estimate $\hat{\boldsymbol{z}}(t)$; therefore, $\boldsymbol{h}(t)$ is bounded. Then the combined error dynamics in Eq. (26) imply that $\dot{\boldsymbol{\xi}}_a(t)$ is bounded. Thus, $\boldsymbol{\xi}_a(t) \in \mathcal{L}_\infty \bigcap \mathcal{L}_2$ and $\dot{\boldsymbol{\xi}}_a(t) \in \mathcal{L}_\infty$. Application of Barbalat's Lemma ensures that $\boldsymbol{\xi}_a(t) \to 0$ as $t \to \infty$ [28]. □

D. Parameter Convergence

In the case of visual measurement, as discussed earlier, $\boldsymbol{y}_c(t)$ depends upon the unknown parameters and hence is not available for the virtual control design in Eq. (20). For the given bounded reference commands $\boldsymbol{R}_c(t)$, one can use the estimated reference input $\hat{\boldsymbol{y}}_c(t)$ in Eq. (20) as follows: $\hat{\boldsymbol{y}}_c(t) = \boldsymbol{R}_c(t)/\hat{b}(t)$, where $\hat{b}(t)$ is obtained from Eq. (31). Note that Theorem 1 is true for any bounded $\boldsymbol{y}_c(t)$ and hence it holds if one replaces $\boldsymbol{y}_c(t)$ with $\hat{\boldsymbol{y}}_c(t)$. Because the objective is the tracking of $\boldsymbol{y}_c(t)$, one needs to ensure that $\hat{\boldsymbol{y}}_c(t)$ converges to $\boldsymbol{y}_c(t)$, which will hold if $\hat{b}(t)$ converges to the true value of b.

From the adaptive law in Eq. (30), it follows that each component of $\hat{\boldsymbol{d}}(t)$ is a nondecreasing function; that is, $\hat{d}_i(t) \geq d_i(0) = 0\,(i = 1, 2, 3)$. From Theorem 1, it follows that $\hat{\boldsymbol{d}}(t)$ is bounded above; therefore, it converges to some finite limit $\bar{\boldsymbol{d}} > 0$ as $t \to \infty$, which need not be the true value of $\boldsymbol{d}_T$. Also, we note that the Lyapunov function $V_1(t)$ is nonincreasing and bounded below, and so it also has a limit as $t \to \infty$. Because all the variables except for $\tilde{b}(t)$ on the right-hand side of Eq. (34) converge to constant values, $\tilde{b}(t)$ also converges. Therefore, $\exists\bar{b}$, such that $\hat{b}(t) \to \bar{b}$ as $t \to \infty$. To ensure that $\bar{b} = b$, a common approach is to introduce an excitation signal in the reference input. In realistic applications, however, a persistently exciting signal is not desirable. Therefore, we use the intelligent excitation technique from [5]. This technique modifies the reference input by adding a sinusoidal signal $k(t)\sin(\omega t)$ to the reference input $R_c(t)$, the amplitude $k(t)$ of which depends on the tracking error as follows:

$$k(t) = \begin{cases} k_0 & t \in [0, T) \\ \min\left[k_1\int_{(j-1)T}^{jT}\|\boldsymbol{\xi}_a(\tau)\|^2\mathrm{d}\tau, k_2 - k_3\right] + k_3 & t \in [jT, (j+1)T) \end{cases} \tag{39}$$

where $k_i > 0$ $(i = 0, 1, 2, 3)$ are design constants, k_3 being a sufficiently small number,[‡] $j = 1, 2, \ldots$, and $T = 2\pi/\omega$. Because the Lyapunov proofs are true for any continuous and bounded reference

[‡]Commonly referred to as the regularization term to ensure boundedness away from zero

input, they are also valid for the modified reference input. The new reference commands are obtained according to $\boldsymbol{y}_c(t) = (1/b)\boldsymbol{R}_c^*(t)$, where $\boldsymbol{R}_c^*(t) = \boldsymbol{R}_c(t) + k(t)\sin(\omega t)\boldsymbol{E}$, and the vector $\boldsymbol{E}$ specifies the direction of the excitation. For instance, we can excite only the reference command in one direction by setting $\boldsymbol{E} = [1 \quad 0 \quad 0]^\top$. As proved in [5], this will guarantee convergence of the estimate $\hat{b}(t)$ to the true value b. Therefore, the estimated reference input $\hat{\boldsymbol{y}}_c(t)$ will converge to the reference input $\boldsymbol{y}_c(t)$, in which $\boldsymbol{R}_c(t)$ is replaced with $\boldsymbol{R}_c(t) + k(t)\sin(\omega t)\boldsymbol{E}$. It is easy to see that $k(t) \to k_3$ as $\boldsymbol{\xi}_a(t) \to 0$. Thus, as the estimation and tracking errors go to zero, the amplitude of the excitation is proportional to k_3. Hence, one can define the *excited* command to be as close to $\boldsymbol{R}_c(t)$ as needed by choosing k_3 to be arbitrarily small.

Remark 2. For the target interception problem, the reference command is $R_c = 0$ and therefore $\boldsymbol{y}_c = 0$. Then the virtual control

$$\boldsymbol{w}_c(t) = -\hat{b}(t)K\hat{\boldsymbol{z}}(t) - S(\boldsymbol{y}_a(t))\hat{\boldsymbol{d}}(t) \tag{40}$$

along with the adaptive laws

$$\begin{aligned} \dot{\hat{b}}(t) &= \rho\,\mathrm{Proj}(\hat{b}(t), -\boldsymbol{y}_a^\top(t)K\hat{\boldsymbol{z}}(t)), \qquad \hat{b}(0) = b_0 > b_{\min} \\ \dot{\hat{\boldsymbol{d}}}(t) &= GS(\boldsymbol{y}_a(t))\boldsymbol{y}_a(t), \qquad \hat{\boldsymbol{d}}(0) = \boldsymbol{0} \end{aligned} \tag{41}$$

guarantees boundedness of all the signals and convergence of the output to zero: $\boldsymbol{y}(t) \to 0$ as $t \to \infty$. There is no need to require parameter convergence, and hence the need for introducing an excitation signal vanishes.

E. Backstepping

We still need to determine the acceleration command $\boldsymbol{a}_F(t)$ to ensure that $\boldsymbol{w}(t)$ tracks the virtual control $\boldsymbol{w}_c(t)$. Recall that $\boldsymbol{w}(t)$ is generated via the filter equation:

$$\dot{\boldsymbol{w}}(t) = \Lambda\boldsymbol{w}(t) - \boldsymbol{a}_F(t) \tag{42}$$

We note that the function $S(\boldsymbol{y}_a)$, and hence the virtual control $\boldsymbol{w}_c(t)$, is not differentiable. Therefore, it cannot be used in the backstepping procedure. One way to circumvent the situation is to replace the discontinuous matrix function $S(\boldsymbol{y}_a)$ with a smooth approximation $S_\chi(\boldsymbol{y}_a)$, which is a diagonal matrix with the entries defined as follows:

$$s_{\chi i}(y_{ai}) = \begin{cases} s_i(y_{ai}) & \boldsymbol{y}_a \notin \Omega_\chi \\ \frac{3}{2\chi}y_{ai} - \frac{1}{2\chi^3}y_{ai}^3 & \boldsymbol{y}_a \in \Omega_\chi \end{cases} \tag{43}$$

where

$$\Omega_\chi = \{\boldsymbol{y}_a\colon |y_{ai}| \le \chi, i = 1, 2, 3\}$$

and $\chi > 0$ is a design parameter. When $|y_{ai}| = \chi$, the following relationships hold

$$s_{\chi i}(y_{ai}) = s_i(y_{ai}), \quad \frac{\partial s_{\chi i}(y_{ai})}{\partial y_{ai}} = \frac{\partial s_i(y_{ai})}{\partial y_{ai}} = 0 \tag{44}$$

Replacing $S(\boldsymbol{y}_a)$ in Eq. (20) with $S_\chi(\boldsymbol{y}_a)$ results in a smooth virtual control:

$$\boldsymbol{w}_c(t) = \hat{b}(t)\boldsymbol{h}(t) - S_\chi(\boldsymbol{y}_a(t))\hat{\boldsymbol{d}}(t) \tag{45}$$

However, this approximation will complicate the backstepping procedure, because its derivative will involve $\dot{\boldsymbol{y}}_a(t)$, and hence $\dot{\boldsymbol{\xi}}_a(t)$, resulting in modifications of the adaptive laws and more complex control architecture. Therefore, we replace $S_\chi(\boldsymbol{y}_a)$ with its filtered version $S_f(t)$, where

$$\dot{S}_f(t) = A_f[S_f(t) - S_\chi(\boldsymbol{y}_a(t))], \qquad S_f(0) = 0 \tag{46}$$

where A_f is a diagonal matrix with the entries $a_{fi} < 0$ ($i = 1, 2, 3$). Because $|s_{\chi i}(y_{ai}(t))| \le 1$ for any $\boldsymbol{y}_a(t)$, the following bound can be written immediately:

$$\begin{aligned} |s_{fi}(t)| &= \left| -\int_0^t \exp[a_{fi}(t-\tau)]a_{fi}s_{\chi i}(y_{ai}(\tau))\,\mathrm{d}\tau \right| \\ &\le 1 - \exp(a_{fi}t) \le 1 \end{aligned} \tag{47}$$

that is, $S_f(t)$ is bounded for any $\boldsymbol{y}_a(t)$. Introducing the error $\boldsymbol{e}_w(t) = \boldsymbol{w}(t) - \boldsymbol{w}_f(t)$, where

$$\boldsymbol{w}_f(t) = \hat{b}(t)\boldsymbol{h}(t) - S_f(t)\hat{\boldsymbol{d}}(t) \tag{48}$$

and using Eq. (14), we obtain

$$\dot{\boldsymbol{e}}_w(t) = \Lambda\boldsymbol{w}(t) - \boldsymbol{a}_F(t) - \dot{\boldsymbol{w}}_f(t) \tag{49}$$

where the continuous signal $\dot{\boldsymbol{w}}_f(t)$ is computed as

$$\begin{aligned} \dot{\boldsymbol{w}}_f(t) = &-\dot{\hat{b}}(t)[-K\hat{\boldsymbol{z}}(t) + KC^\top\boldsymbol{y}_c(t)] - \hat{b}(t)[-K\dot{\hat{\boldsymbol{z}}}(t) \\ &+ KC^\top\dot{\boldsymbol{y}}_c(t)] - S_f(t)\dot{\hat{\boldsymbol{d}}}(t) + A_f[S_f(t) - S_\chi(\boldsymbol{y}_a(t))]\hat{\boldsymbol{d}}(t) \end{aligned} \tag{50}$$

and is available for feedback. Therefore, the guidance law $\boldsymbol{a}_F(t)$ can be designed as

$$\boldsymbol{a}_F(t) = \Lambda\boldsymbol{w}_f(t) - \dot{\boldsymbol{w}}_f(t) + \boldsymbol{y}_a(t) \tag{51}$$

so that the filter error dynamics reduce to

$$\dot{\boldsymbol{e}}_w(t) = \Lambda\boldsymbol{e}_w(t) - \boldsymbol{y}_a(t) \tag{52}$$

Because

$$\boldsymbol{w}(t) - \boldsymbol{w}_c(t) = \boldsymbol{e}_w(t) - S_f(t)\hat{\boldsymbol{d}}(t) + S(\boldsymbol{y}_a(t))\hat{\boldsymbol{d}}(t)$$

the error dynamics in Eq. (26) can be written in the following form:

$$\begin{aligned} \dot{\boldsymbol{\xi}}_a(t) = &A_a\boldsymbol{\xi}_a(t) + \frac{1}{b}B_a[\tilde{b}(t)\boldsymbol{h}(t) + \boldsymbol{d}(t) \\ &- S(\boldsymbol{y}_a(t))\hat{\boldsymbol{d}}(t) + \boldsymbol{w}(t) - \boldsymbol{w}_c(t)] = A_a\boldsymbol{\xi}_a(t) \\ &+ \frac{1}{b}B_a(\tilde{b}(t)\boldsymbol{h}(t) + \boldsymbol{d}(t) - S_f(t)\hat{\boldsymbol{d}}(t) + \boldsymbol{e}_w(t)) \end{aligned} \tag{53}$$

Here, we can prove only ultimate boundedness of the state estimation and tracking errors, provided that the parameter errors remain bounded. The projection operator in Eq. (31) guarantees boundedness of $\hat{b}(t)$, and therefore $\tilde{b}(t)$ is bounded. To ensure boundedness of $\hat{\boldsymbol{d}}(t)$, and hence of the error $\tilde{\boldsymbol{d}}(t)$, we have to modify the adaptive law in Eq. (31). Here, we again choose a projection-based adaptive law,

$$\dot{\hat{\boldsymbol{d}}}(t) = G\mathrm{Proj}(\hat{\boldsymbol{d}}(t), S(\boldsymbol{y}_a(t))\boldsymbol{y}_a(t)), \qquad \hat{\boldsymbol{d}}(0) = \boldsymbol{0} \tag{54}$$

that guarantees the inequalities [30]:

$$\begin{aligned} &\|\hat{\boldsymbol{d}}(t)\| \le d_{\max} \\ &\tilde{\boldsymbol{d}}^\top(t)[-S(\boldsymbol{y}_a(t))\boldsymbol{y}_a(t) + \mathrm{Proj}(\hat{\boldsymbol{d}}(t), S(\boldsymbol{y}_a(t))\boldsymbol{y}_a(t))] \le 0 \end{aligned} \tag{55}$$

Theorem 2. The guidance law in Eq. (51), along with the adaptive laws in Eqs. (31) and (54), guarantees uniform ultimate boundedness of all error signals in the systems in Eqs. (52) and (53).

Proof. Because $S_f(t)$ is always bounded due to its definition, we consider the following Lyapunov function candidate independent of $S_f(t)$:

$$\begin{aligned} V_2(\boldsymbol{\xi}_a(t), \tilde{b}(t), \tilde{\boldsymbol{d}}(t), \boldsymbol{e}_w(t)) = &\boldsymbol{\xi}_a^\top(t)P_a\boldsymbol{\xi}_a(t) \\ &+ \frac{1}{b}\left[\frac{\tilde{b}^2(t)}{\rho} + \tilde{\boldsymbol{d}}^\top(t)G^{-1}\tilde{\boldsymbol{d}}(t)\right] + \frac{1}{b}\boldsymbol{e}_w^\top(t)\boldsymbol{e}_w(t) \end{aligned} \tag{56}$$

Its derivative along the solutions of the systems in Eqs. (26), (52), and (53) can be computed following the same steps as in the previous Proof.

$$\begin{aligned}\dot{V}_2(t) &= \boldsymbol{\xi}_a^\top(t)[A_a^\top P_a + P_a A_a]\boldsymbol{\xi}_a(t)\\ &+ \frac{2}{b}\left[\frac{\tilde{b}(t)}{\rho}\dot{\tilde{b}}(t) + \tilde{\boldsymbol{d}}^\top(t)G^{-1}\dot{\tilde{\boldsymbol{d}}}(t)\right]\\ &+ 2\boldsymbol{\xi}_a^\top(t)P_a\frac{1}{b}B_a[\tilde{b}(t)\boldsymbol{h}(t) + \boldsymbol{d}(t) - S_f(t)\hat{\boldsymbol{d}}(t) + \boldsymbol{e}_w(t)]\\ &- \frac{2}{b}\boldsymbol{e}_w^\top(t)\Lambda\boldsymbol{e}_w(t) = -\boldsymbol{\xi}_a^\top(t)Q_a\boldsymbol{\xi}_a(t)\\ &+ \frac{2\tilde{b}(t)}{b}\left[\boldsymbol{y}_a^\top(t)\boldsymbol{h}(t) + \frac{1}{\rho}\dot{\tilde{b}}(t)\right] + \frac{2}{b}\tilde{\boldsymbol{d}}^\top(t)[-S(\boldsymbol{y}_a(t))\boldsymbol{y}_a(t)\\ &+ G^{-1}\dot{\tilde{\boldsymbol{d}}}(t)] + \frac{2}{b}\boldsymbol{\xi}_a^\top(t)P_a B_a[\boldsymbol{d}(t) - S(\boldsymbol{y}_a(t))\boldsymbol{d}_T]\\ &+ \frac{2}{b}\boldsymbol{y}_a^\top(t)[S(\boldsymbol{y}_a(t)) - S_\chi(\boldsymbol{y}_a(t)) + S_\chi(\boldsymbol{y}_a(t)) - S_f(t)]\hat{\boldsymbol{d}}(t)\\ &- \frac{2}{b}\boldsymbol{e}_w^\top(t)\Lambda\boldsymbol{e}_w(t) \le -\boldsymbol{\xi}_a^\top(t)Q_a\xi_a(t) - \frac{2}{b}\boldsymbol{e}_w^\top(t)\Lambda\boldsymbol{e}_w(t)\\ &+ \frac{2}{b}\boldsymbol{y}_a^\top(t)[S(\boldsymbol{y}_a(t)) - S_\chi(\boldsymbol{y}_a(t)) + S_\chi(\boldsymbol{y}_a(t)) - S_f(t)]\hat{\boldsymbol{d}}(t)\end{aligned} \tag{57}$$

Outside the compact set Ω_χ, we have $S(\boldsymbol{y}_a) = S_\chi(\boldsymbol{y}_a)$ and $\dot{S}_\chi(\boldsymbol{y}_a(t)) = 0$. Therefore, with the notation $E_S(t) = S_f(t) - S_\chi(\boldsymbol{y}_a(t))$, Eq. (46) reduces to

$$\dot{E}_S(t) = A_f E_S(t) \tag{58}$$

the solution of which can be written as $E_S(t) = \exp(A_f t)E_S(0)$. The following bound can be immediately derived:

$$\|E_S(t)\|_F \le \exp(a_f t)\|E_S(0)\|_F \tag{59}$$

where $a_f = \max\{a_{fi}, i = 1, 2, 3\}$. Therefore, the derivative of the Lyapunov function candidate in Eq. (56) can be upper-bounded as follows:

$$\begin{aligned}\dot{V}_2(t) &\le -\lambda_{\min}(Q_a)\|\boldsymbol{\xi}_a(t)\|^2 - \frac{\bar{\lambda}}{b}\|\boldsymbol{e}_w(t)\|^2\\ &+ \frac{2d_{\max}}{b}\exp(a_f t)\|\boldsymbol{\xi}_a(t)\|\|E_S(0)\|_F\end{aligned} \tag{60}$$

where $\bar{\lambda} = \min\{\lambda_1, \lambda_2, \lambda_3\}$ and $d_{\max}$ is the bound for the estimate $\hat{\boldsymbol{d}}(t)$, guaranteed by the projection operator. Completing the squares in Eq. (60) results in

$$\dot{V}_2(t) \le -[\lambda_{\min}(Q_a) - c_1^2]\|\boldsymbol{\xi}_a(t)\|^2 - \frac{\bar{\lambda}}{b}\|\boldsymbol{e}_w(t)\|^2 + c_2\exp(2a_f t) \tag{61}$$

where c_1 is chosen such that $\lambda_{\min}(Q_a) - c_1^2 > 0$ and $c_2 = (bc_1)^{-2}d_{\max}^2 \| E_S(0) \|_F^2$. From the relationship in Eq. (61), it follows that $\dot{V}_2(t) \le 0$ outside the compact set:

$$\Omega_1 = \left\{\|\boldsymbol{\xi}_a\| \le \sqrt{\frac{c_2}{\lambda_{\min}(Q_a) - c_1^2}}, \boldsymbol{e}_w = \boldsymbol{0}, |\tilde{b}| \le \tilde{b}^*, \|\tilde{\boldsymbol{d}}\| \le \tilde{d}^*\right\} \tag{62}$$

where the bounds $\tilde{b}^*$ and $\tilde{d}^*$ are guaranteed by the projection operator. Thus, the error signals $\boldsymbol{\xi}_a(t)$, $\tilde{b}(t)$, $\tilde{\boldsymbol{d}}(t)$, and $\boldsymbol{e}_w(t)$ are uniformly ultimately bounded. Rearranging the terms in Eq. (61) and integrating, we obtain

$$\begin{aligned}&\int_0^t\left\{\left[\lambda_{\min}(Q_a) - c_1^2\right]\|\boldsymbol{\xi}_a(\tau)\|^2 + \frac{\lambda}{b}\|\boldsymbol{e}_w(\tau)\|^2\right\}\mathrm{d}\tau\\ &\le V_2(0) - V_2(t) + \int_0^t c_2\exp(2a_f\tau)\,\mathrm{d}\tau < \infty\end{aligned} \tag{63}$$

Thus, $\boldsymbol{\xi}_a(t) \in \mathcal{L}_2(\mathbb{R}^6)\bigcap\mathcal{L}_\infty(\mathbb{R}^6)$ and $\boldsymbol{e}_w(t) \in \mathcal{L}_2(\mathbb{R}^3)\bigcap\mathcal{L}_\infty(\mathbb{R}^3)$. Also, from the boundedness of error signals and reference commands, it follows that $\boldsymbol{h}(t)$ is bounded. Because the matrix $S_f(t)$ is bounded, it follows that $\boldsymbol{w}_f(t)$ and $\dot{\boldsymbol{w}}_f(t)$ are bounded and therefore $\boldsymbol{a}_F(t)$ is bounded. Then the error dynamics in Eqs. (52) and (53) imply that $\dot{\boldsymbol{\xi}}_a(t) \in \mathcal{L}_\infty(\mathbb{R}^6)$ and $\dot{\boldsymbol{e}}_w(t) \in \mathcal{L}_\infty(\mathbb{R}^3)$. Application of Barbalat's Lemma ensures that $\boldsymbol{\xi}_a(t) \to 0$ and $\boldsymbol{e}_w(t) \to 0$ as $t \to \infty$ [28]. Therefore, there exists a time instant $t_\chi > 0$ such that $\boldsymbol{y}_a(t_\chi)$ enters the set Ω_χ and remains inside thereafter for $t \ge t_\chi$ for arbitrary χ selected in Eq. (43).

Inside the compact set Ω_χ, we have

$$2\boldsymbol{y}_a^\top(t)[S(\boldsymbol{y}_a) - S_\chi(\boldsymbol{y}_a)]\hat{\boldsymbol{d}}(t) = \chi\sum_{i=1}^{3}\left[2\frac{|y_{ai}|}{\chi} - 3\frac{|y_{ai}^2|}{\chi^2} + \frac{|y_{ai}|^4}{\chi^4}\right]\hat{d}_i(t) \tag{64}$$

The term in the square bracket in Eq. (64) is positive for $|y_{ai}(t)| \le \chi$ and has a maximum value of $c_3 = \frac{1}{4}(6\sqrt{3} - 9)$. Therefore,

$$2\boldsymbol{y}_a^\top(t)[S(\boldsymbol{y}_a(t)) - S_\chi(\boldsymbol{y}_a(t))]\hat{\boldsymbol{d}}(t) \le c_4\chi \tag{65}$$

where $c_4 = 3c_3 d_{\max}$. By definition, $\|S_\chi(\boldsymbol{y}_a(t))\|_F \le \sqrt{3}$ for any $t \ge 0$, therefore, it follows from Eq. (46)

$$\|E_S(t)\|_F = \left\|-\int_0^t e^{A_f(t-\tau)}A_f S_\chi(\boldsymbol{y}_a(\tau))\,\mathrm{d}\tau - S_\chi(\boldsymbol{y}_a(t))\right\|_F \le 2\sqrt{3} \tag{66}$$

Therefore, inside the set Ω_χ, the derivative of $V_2(t)$ can be further upper-bounded as follows:

$$\begin{aligned}\dot{V}_2(t) &\le -\lambda_{\min}(Q_a)\|\boldsymbol{\xi}_a(t)\|^2 + c_4\chi + 2c_5\|\boldsymbol{\xi}_a(t)\| - \frac{\lambda}{b}\|\boldsymbol{e}_w(t)\|^2\\ &\le -\left[\lambda_{\min}(Q_a) - c_6^2\right]\|\boldsymbol{\xi}_a(t)\|^2 + \frac{c_5^2}{c_6^2} + c_4\chi - \frac{\lambda}{b}\|\boldsymbol{e}_w(t)\|^2\end{aligned} \tag{67}$$

where $c_5 = 2\sqrt{3}d_{\max}$ and c_6 is chosen such that $c_7 = \lambda_{\min}(Q_a) - c_6^2 > 0$. The inequality in Eq. (67) implies that $\dot{V}_2(t) \le 0$ outside the compact set:

$$\Omega_2 = \left\{\|\boldsymbol{\xi}_a\| \le \sqrt{\frac{c_8}{c_7}}, \boldsymbol{e}_w = \boldsymbol{0}, |\tilde{b}| \le \tilde{b}^*, |\tilde{\boldsymbol{d}}| \le \tilde{d}^*\right\} \tag{68}$$

where $c_8 = (c_5^2/c_6^2) + c_4\chi$. Thus, the trajectories of the closed-loop system in Eqs. (31) and (52–54) are uniformly ultimately bounded. Decreasing the parameter χ will decrease the size of the set Ω_χ and hence the bounds on the components of the output tracking error $\boldsymbol{e}_c(t)$. However, the bounds on the remaining components of $\boldsymbol{\xi}_a(t)$ that are in the null space of C_a are not affected directly and are defined by the ultimate bound of the closed-loop system, which can be determined following the steps in [19]. □

IV. Robustness to Measurement Noise

A. Measurement Noise Definition

The guidance law derived in the previous section assumes availability of perfect measurements from the visual sensor. However, in realistic applications, these measurements are corrupted by noise. Therefore, instead of the ideal measurements $y_I(t)$, $z_I(t)$, and $b_I(t)$, one should consider

$$\begin{aligned}y_I^*(t) = y_I(t) + n_y(t), \qquad z_I^*(t) = z_I(t) + n_z(t)\\ b_I^*(t) = b_I(t) + n_b(t)\end{aligned} \tag{69}$$

where $\boldsymbol{n}_I(t) \triangleq [\,n_y(t) \quad n_z(t) \quad n_b(t)\,]^\top$ represents the vector of the noise components in the corresponding measurements. In this section, we analyze the performance of the derived guidance law in the preceding section in the presence of noisy measurements $y_I^*(t)$, $z_I^*(t)$, and $b_I^*(t)$. In this case, the expressions in Eqs. (6) and (7) take the form

$$\tan\lambda^*(t) = \frac{y_I(t) + n_y(t)}{l}$$
$$\tan\vartheta^*(t) = \frac{z_I(t) + n_z(t)}{\sqrt{l^2 + [y_I(t) + n_y(t)]^2}} \tag{70}$$
$$a_I^*(t) = \frac{\sqrt{l^2 + [y_I(t) + n_y(t)]^2 + [z_I(t) + n_z(t)]^2}}{b_I(t) + n_b(t)}$$

The measurements of the scaled state vector $\boldsymbol{r}(t)$ are expressed in the following form:

$$\boldsymbol{r}^*(t) = L_{E/B} a_I^*(t) \boldsymbol{T}_{BI}^*(\lambda^*(t), \vartheta^*(t)) \triangleq L_{E/B} \boldsymbol{f}(y_I^*(t), z_I^*(t), b_I^*(t)) \tag{71}$$

where the vector $\boldsymbol{T}_{BI}^*(\lambda^*(t), \vartheta^*(t))$ is defined similar to $\boldsymbol{T}_{BI}$ in Eq. (8), with λ and ϑ replaced with λ^* and ϑ^*, respectively. When the noise level is small, one can expand the expressions in Eq. (71) into a Taylor series around the ideal measurements $y_I(t)$, $z_I(t)$, and $b_I(t)$:

$$\boldsymbol{r}^*(t) = \boldsymbol{r}(t) + L_{E/B} \nabla \boldsymbol{f}(y_I(t), z_I(t), b_I(t)) \boldsymbol{n}_I(t) \tag{72}$$

where $\nabla \boldsymbol{f}(y_I, z_I, b_I)$ is the Jacobian of the vector function $\boldsymbol{f}(y_I, z_I, b_I)$ with respect to arguments y_I, z_I, and b_I. For the uncorrelated zero-mean Gaussian white noise $\boldsymbol{n}_I(t)$ with the correlation matrix,

$$E\{\boldsymbol{n}_I(t)\boldsymbol{n}_I^\top(\tau)\} = K_{\boldsymbol{n}_I}\delta(t-\tau)$$

where $E\{\cdot\}$ denotes the mathematical expectation

$$K_{\boldsymbol{n}_I} = \begin{bmatrix} \bar{n}_y & 0 & 0 \\ 0 & \bar{n}_z & 0 \\ 0 & 0 & \bar{n}_b \end{bmatrix}$$

with $\bar{n}_y$, $\bar{n}_z$, and $\bar{n}_b$ being positive constants; $\delta(\cdot)$ is the Dirac delta function; the vector

$$\boldsymbol{n}_r(t) = L_{E/B} \nabla \boldsymbol{f}(y_I(t), z_I(t), b_I(t)) \boldsymbol{n}_I(t) \tag{73}$$

also represents a zero-mean Gaussian white-noise process with the correlation matrix

$$E\{\boldsymbol{n}_r(t)\boldsymbol{n}_r^\top(\tau)\} = S_n(t) K_{\boldsymbol{n}_I} S_n^\top(\tau)\delta(t-\tau) \tag{74}$$

where

$$S_n(t) = L_{E/B}(t) \nabla \boldsymbol{f}(y_I(t), z_I(t), b_I(t)) \tag{75}$$

Therefore, in the sequel, we will assume that the scaled state vector $\boldsymbol{r}(t)$ is available with the additive, zero-mean, Gaussian white noise

$$\boldsymbol{r}^*(t) = \boldsymbol{r}(t) + \boldsymbol{n}_r(t) \tag{76}$$

with the correlation matrix

$$E\{\boldsymbol{n}_r(t)\boldsymbol{n}_r^\top(\tau)\} = K_{\boldsymbol{n}_r}(t,\tau)\delta(t-\tau) \tag{77}$$

where $K_{\boldsymbol{n}_r}(t,\tau) > 0$ for all t, and $\tau > 0$.

B. Error Dynamics Modification

First we note that the observer dynamics in Eq. (21) will be driven by the noisy measurement

$$\boldsymbol{y}^*(t) = \boldsymbol{r}^*(t) = \boldsymbol{y}(t) + \boldsymbol{n}_r(t)$$

instead of $\boldsymbol{y}(t)$. So the observer dynamics are written as follows:

$$\dot{\hat{\boldsymbol{z}}}^*(t) = A_m \hat{\boldsymbol{z}}^*(t) + B_m \hat{\boldsymbol{y}}_c(t) + L[\boldsymbol{y}^*(t) - \hat{\boldsymbol{y}}^*(t)]$$
$$\hat{\boldsymbol{y}}^*(t) = C\hat{\boldsymbol{z}}^*(t) \tag{78}$$

where L is the observer gain matrix that satisfies the SPR and Hurwitz requirements. In the guidance law in Eq. (51) and in Eqs. (43), (46), (48), and (50), the ideal measurement $\boldsymbol{y}(t)$ will be replaced with $\boldsymbol{y}^*(t)$. For clarity, we present the complete guidance law:

$$\begin{aligned} \boldsymbol{a}_F(t) &= \Lambda \boldsymbol{w}_f^*(t) - \dot{\boldsymbol{w}}_f^*(t) + \boldsymbol{y}_a^*(t) \\ \boldsymbol{w}_f^*(t) &= \hat{b}(t)\boldsymbol{h}^*(t) - S_f^*(t)\hat{\boldsymbol{d}}(t) \\ \boldsymbol{h}^*(t) &= -K\hat{\boldsymbol{z}}^*(t) + KC^\top \hat{\boldsymbol{y}}_c(t) \\ \dot{S}_f^*(t) &= A_f(S_f^*(t) - S_\chi(\boldsymbol{y}_a^*(t))) \end{aligned} \tag{79}$$

where $S_\chi(\boldsymbol{y}_a^*)$ is defined according to Eqs. (27) and (43), with $\boldsymbol{y}_a(t)$ being replaced with $\boldsymbol{y}_a^*(t)$, the latter being defined as follows:

$$\begin{aligned} \boldsymbol{y}_a^* = C_a\boldsymbol{\xi}_a^* &= C\boldsymbol{e}^* + C\tilde{\boldsymbol{z}}^* = \boldsymbol{y}^* - \boldsymbol{y}_m + \boldsymbol{y}^* - \hat{\boldsymbol{y}}^* = \boldsymbol{e}_c \\ &+ \boldsymbol{n}_r + \tilde{\boldsymbol{y}} + \boldsymbol{n}_r = C_a\boldsymbol{\xi}_a + 2\boldsymbol{n}_r = \boldsymbol{y}_a + 2\boldsymbol{n}_r \end{aligned} \tag{80}$$

The adaptive laws are modified by replacing $\boldsymbol{y}_a(t)$ with $\boldsymbol{y}_a^*(t)$ and $\boldsymbol{h}(t)$ with $\boldsymbol{h}^*(t)$:

$$\begin{aligned} \dot{\hat{b}}(t) &= \rho \mathrm{Proj}(\hat{b}(t), -\boldsymbol{y}_a^{*\top}(t)\boldsymbol{h}^*(t)), \qquad \hat{b}(0) = b_0 > b_{\min} \\ \dot{\hat{\boldsymbol{d}}}(t) &= G\mathrm{Proj}(\hat{\boldsymbol{d}}(t), S(\boldsymbol{y}_a^*)\boldsymbol{y}_a^*(t)), \qquad \hat{\boldsymbol{d}}(0) = \boldsymbol{0} \end{aligned} \tag{81}$$

The error dynamics in Eqs. (25) and (52) now take the form

$$\begin{aligned} \dot{\boldsymbol{\xi}}_a(t) &= A_a\boldsymbol{\xi}_a(t) \\ &+ \frac{1}{b}B_a[\tilde{b}(t)\boldsymbol{h}^*(t) + \boldsymbol{d}(t) - S_f^*(t)\hat{\boldsymbol{d}}(t) + \boldsymbol{e}_w(t)] - D_a\boldsymbol{n}_r(t) \\ \dot{\boldsymbol{e}}_w(t) &= -\Lambda\boldsymbol{e}_w(t) - \boldsymbol{y}_a^*(t) \\ \boldsymbol{y}_a^*(t) &= C_a\boldsymbol{\xi}_a(t) + 2\boldsymbol{n}_r(t) \end{aligned} \tag{82}$$

where $D_a = [\,0_{3\times 6} \quad L^\top\,]^\top$.

C. Stability Analysis

Now we show that the error system in Eqs. (81) and (82) is ultimately bounded for any bounded $\boldsymbol{n}_r(t)$, for which the solution exists.

Theorem 3. For any bounded $\boldsymbol{n}_r(t)$, the guidance law in Eq. (79), along with the adaptive laws in Eq. (81), guarantees the uniform ultimate boundedness of the error signals $\boldsymbol{\xi}_a(t)$, $\tilde{b}(t)$ *and* $\tilde{\boldsymbol{d}}(t)$.

Proof. Consider the Lyapunov function candidate:

$$\begin{aligned} V_3(\boldsymbol{\xi}_a(t), \tilde{b}(t), \tilde{\boldsymbol{d}}(t), \boldsymbol{e}_w(t)) &= \boldsymbol{\xi}_a^\top(t)P_a\boldsymbol{\xi}_a(t) \\ &+ \frac{1}{b}\left[\frac{\tilde{b}^2(t)}{\rho} + \tilde{\boldsymbol{d}}^\top(t)G^{-1}\tilde{\boldsymbol{d}}(t) + \boldsymbol{e}_w^\top(t)\boldsymbol{e}_w(t)\right] \end{aligned} \tag{83}$$

The derivative of $V_3(t)$ along the trajectories of the systems in Eqs. (81) and (82) can be computed as follows:

$$\begin{aligned} \dot{V}_3(t) &= \boldsymbol{\xi}_a^\top(t)(A_a^\top P_a + P_a A_a)\boldsymbol{\xi}_a(t) - 2\boldsymbol{\xi}_a^\top(t)P_aD_a\boldsymbol{n}_r(t) \\ &+ \frac{2}{b}\boldsymbol{\xi}_a^\top(t)P_aB_a[\tilde{b}(t)\boldsymbol{h}^*(t) + \boldsymbol{d}(t) - S_f^*(t)\hat{\boldsymbol{d}}(t) + \boldsymbol{e}_w(t)] \\ &+ \frac{2}{b}\left(\frac{\tilde{b}(t)}{\rho}\dot{\tilde{b}}(t) + \tilde{\boldsymbol{d}}^\top(t)G^{-1}\dot{\tilde{\boldsymbol{d}}}(t) + \boldsymbol{e}_w^\top(t)\dot{\boldsymbol{e}}_w(t)\right) \\ &= -\boldsymbol{\xi}_a^\top(t)Q_a\boldsymbol{\xi}_a(t) + \frac{2\tilde{b}(t)}{b}\left[\boldsymbol{y}_a^{*\top}(t)\boldsymbol{h}^*(t) + \frac{1}{\rho}\dot{\tilde{b}}(t)\right] \\ &+ \frac{2\tilde{b}(t)}{b}\tilde{\boldsymbol{d}}^\top(t)[-S(\boldsymbol{y}_a^*)\boldsymbol{y}_a^*(t) + G^{-1}\dot{\tilde{\boldsymbol{d}}}(t)] - \frac{4}{b}\boldsymbol{n}_r^\top(t)[\tilde{b}(t)\boldsymbol{h}^*(t) \\ &+ \boldsymbol{d}(t) - S(\boldsymbol{y}_a^*)\hat{\boldsymbol{d}}(t) + \boldsymbol{e}_w^*(t)] - 2\boldsymbol{\xi}_a^\top(t)P_aD_a\boldsymbol{n}_r(t) \\ &+ \frac{2}{b}\boldsymbol{y}_a^{*\top}(t)[\boldsymbol{d}(t) - S(\boldsymbol{y}_a^*)\boldsymbol{d}_T] + \frac{2}{b}\boldsymbol{y}_a^\top(t)[S(\boldsymbol{y}_a^*) - S_f^*(t)]\hat{\boldsymbol{d}}(t) \\ &- \frac{2}{b}\boldsymbol{e}_w^\top(t)\Lambda\boldsymbol{e}_w(t) \end{aligned} \tag{84}$$

Upon substitution of the adaptive laws from Eq. (81) into Eq. (84) and using the properties of the projection operator from Eqs. (33) and (55), we conclude that

$$\begin{aligned}\dot{V}_3(t) \le & -\boldsymbol{\xi}_a^{*\top}(t)Q_a\boldsymbol{\xi}_a^*(t) - \frac{2}{b}\boldsymbol{e}_w^\top(t)\Lambda\boldsymbol{e}_w(t) - \frac{4}{b}\boldsymbol{n}_r^\top(t)[\tilde{b}(t)\boldsymbol{h}^*(t) \\ & + \boldsymbol{d}(t) - S(\boldsymbol{y}^*)\hat{\boldsymbol{d}}(t) + \boldsymbol{e}_w(t)] - 2\boldsymbol{\xi}_a^\top(t)P_aD_a\boldsymbol{n}_r(t) \\ & + \frac{2}{b}\boldsymbol{y}_a^{*\top}(t)[\boldsymbol{d}(t) - S(\boldsymbol{y}_a^*)\boldsymbol{d}_T] + \frac{2}{b}\boldsymbol{y}_a^\top(t)[S(\boldsymbol{y}_a^*) - S_f^*(t)]\hat{\boldsymbol{d}}(t)\end{aligned} \tag{85}$$

Taking into account the relationship

$$\boldsymbol{y}_a^{*\top}(t)\boldsymbol{d}(t) - \boldsymbol{y}_a^{*\top}(t)S(\boldsymbol{y}_a^*)\boldsymbol{d}_T = \sum_{i=1}^{3}[y_{ai}^*(t)d_i(t) - |y_{ai}^*(t)|d_{Ti}] \le 0 \tag{86}$$

the inequality in Eq. (85) can be reduced to

$$\begin{aligned}\dot{V}_3(t) \le & -\boldsymbol{\xi}_a^\top(t)Q_a\boldsymbol{\xi}_a(t) - 2\boldsymbol{\xi}_a^\top(t)P_aD_a\boldsymbol{n}_r(t) - \frac{4}{b}\boldsymbol{n}_r^\top(t)[\tilde{b}(t)\boldsymbol{h}^*(t) \\ & + \boldsymbol{d}(t) - S(\boldsymbol{y}^*)\hat{\boldsymbol{d}}(t) + \boldsymbol{e}_w(t)] + \frac{2}{b}\boldsymbol{y}_a^\top(t)[S(\boldsymbol{y}_a^*) - S_f^*(t)]\hat{\boldsymbol{d}}(t) \\ & - \frac{2}{b}\boldsymbol{e}_w^\top(t)\Lambda\boldsymbol{e}_w(t)\end{aligned} \tag{87}$$

The first square bracketed term in Eq. (87) can be upper-bounded by the norm of the error signals $\boldsymbol{\xi}_a(t)$ and $\boldsymbol{e}_w(t)$ as follows:

$$\begin{aligned}&\|\tilde{b}(t)\boldsymbol{h}^*(t) + \boldsymbol{d}(t) - S(\boldsymbol{y}^*)\hat{\boldsymbol{d}}(t) + \boldsymbol{e}_w(t)\| \\ &\quad \le \|\boldsymbol{e}_w(t)\| + c_8\|\boldsymbol{\xi}_a(t)\| + c_9\end{aligned} \tag{88}$$

where c_8 and c_9 are positive constants. Indeed, the inequalities in Eqs. (33) and (55) imply boundedness of the signals $\tilde{b}(t)$ and $\hat{\boldsymbol{d}}(t)$ by some constants $\tilde{b}^*$ and $\tilde{d}^*$, respectively; the signal $\boldsymbol{d}(t)$ is bounded by the assumption; and $S(\boldsymbol{y}^*)$ is bounded by the definition in Eq. (27). From the relationship

$$\hat{\boldsymbol{z}}^*(t) = \boldsymbol{z}(t) - \tilde{\boldsymbol{z}}(t) = \boldsymbol{z}_m(t) + \boldsymbol{e}(t) - \tilde{\boldsymbol{z}}(t)$$

it follows that

$$\|\boldsymbol{h}^*(t)\| \le \|K\|_F[\|\boldsymbol{\xi}_a(t)\| + \|\boldsymbol{z}_m(t)\|] + \|KC^\top\hat{\boldsymbol{y}}_c(t)\|$$

From the boundedness of $\hat{\boldsymbol{y}}_c(t)$ and $\boldsymbol{z}_m(t)$, it follows that there exist positive constants c_8 and c_9 such that Eq. (88) holds. Therefore, $\dot{V}_3(t)$ can be further upper-bounded as follows:

$$\begin{aligned}\dot{V}_3(t) \le & -\lambda_{\min}(Q_a)\|\boldsymbol{\xi}_a(t)\|^2 - \frac{2}{b}\lambda_{\min}(\Lambda)\|\boldsymbol{e}_w(t)\|^2 \\ & + \frac{4}{b}\|\boldsymbol{n}_r(t)\|[\|\boldsymbol{e}_w(t)\| + c_8\|\boldsymbol{\xi}_a(t)\| + c_9] \\ & - 2\|P_aD_a\|_F\|\boldsymbol{\xi}_a(t)\|\|\boldsymbol{n}_r(t)\| + \frac{2}{b}\boldsymbol{y}_a^\top(t)[S(\boldsymbol{y}_a^*) - S_f^*(t)]\hat{\boldsymbol{d}}(t)\end{aligned} \tag{89}$$

Recall that for $\boldsymbol{y}_a^* \notin \Omega_\chi$, we have $S(\boldsymbol{y}_a^*) = S_\chi(\boldsymbol{y}_a^*)$ and the inequality in Eq. (59) holds, whereas for $\boldsymbol{y}_a^* \in \Omega_\chi$, the inequality in Eq. (66) holds. Therefore, $\dot{V}_3(t)$ can be further upper-bounded as follows. For $\boldsymbol{y}_a^* \notin \Omega_\chi$,

$$\begin{aligned}\dot{V}_3(t) \le & -\lambda_{\min}(Q_a)\|\boldsymbol{\xi}_a(t)\|^2 - \frac{2}{b}\lambda_{\min}(\Lambda)\|\boldsymbol{e}_w(t)\|^2 \\ & + \frac{4}{b}\|\boldsymbol{n}_r(t)\|[\|\boldsymbol{e}_w(t)\| + c_8\|\boldsymbol{\xi}_a(t)\| + c_9] \\ & + 2\|P_aD_a\|_F\|\boldsymbol{\xi}_a(t)\|\|\boldsymbol{n}_r(t)\| + 2c_{10}\exp(a_ft)\|\boldsymbol{\xi}_a(t)\|\end{aligned} \tag{90}$$

where $c_{10} = d_{\max}\|E_S(0)\|_F/b$. Completing the squares in Eq. (90) yields

$$\begin{aligned}\dot{V}_3(t) \le & -\left[\lambda_{\min}(Q_a) - c_{11}^2 - c_{12}^2\right]\|\boldsymbol{\xi}_a(t)\|^2 \\ & - \left[\frac{2}{b}\lambda_{\min}(\Lambda) - c_{13}^2\right]\|\boldsymbol{e}_w(t)\|^2 + \frac{4c_9}{b}\|\boldsymbol{n}_r(t)\| \\ & + c_{14}\|\boldsymbol{n}_r(t)\|^2 + \frac{c_{10}^2}{c_{12}^2}\exp(2a_ft)\end{aligned} \tag{91}$$

where the constants c_{11}, c_{12}, and c_{13} are chosen such that

$$c_{15} = \lambda_{\min}(Q_a) - c_{11}^2 - c_{12}^2 > 0, \qquad \frac{2}{b}\lambda_{\min}(\Lambda) - c_{13}^2 > 0$$

and c_{14} denotes the constant

$$c_{14} = \frac{1}{b^2}\left[\frac{(2c_8 + b\|P_aD_a\|_F)^2}{c_{11}^2} + \frac{4}{c_{13}^2}\right]$$

The inequality in Eq. (91) implies that $\dot{V}_3(t) \le 0$ outside the compact set:

$$\Omega_2 = \left\{\|\boldsymbol{\xi}_a\| \le \sqrt{\frac{c_{16}}{c_{15}}}, \boldsymbol{e}_w = \boldsymbol{0}, |\tilde{b}| \le \tilde{b}^*, \|\tilde{\boldsymbol{d}}\| \le \tilde{d}^*\right\} \tag{92}$$

where

$$c_{16} = c_{14}c_{17}^2 + \frac{4c_9}{b}c_{17} + \frac{c_{10}^2}{c_{12}^2}$$

with c_{17} being the norm bound of $\boldsymbol{n}_r(t)$. Thus, the signals $\boldsymbol{\xi}_a(t)$, $\tilde{b}(t)$, $\tilde{\boldsymbol{d}}(t)$, and $\boldsymbol{e}_w(t)$ are uniformly ultimately bounded. For $\boldsymbol{y}_a^* \in \Omega_\chi$, we have the inequality

$$\begin{aligned}\dot{V}_3(t) \le & -\lambda_{\min}(Q_a)\|\boldsymbol{\xi}_a(t)\|^2 - \frac{2}{b}\lambda_{\min}(\Lambda)\|\boldsymbol{e}_w(t)\|^2 \\ & + \frac{4}{b}\|\boldsymbol{n}_r(t)\|[\|\boldsymbol{e}_w(t)\| + c_8\|\boldsymbol{\xi}_a(t)\| + c_9] \\ & + 2\|P_aD_a\|_F\|\boldsymbol{\xi}_a(t)\|\|\boldsymbol{n}_r(t)\| + \frac{2}{b}\sqrt{3}d_{\max}\|\boldsymbol{\xi}_a(t)\|\end{aligned} \tag{93}$$

which, upon completion of the squares, yields

$$\begin{aligned}\dot{V}_3(t) \le & -\left[\lambda_{\min}(Q_a) - c_{11}^2 - c_{12}^2\right]\|\boldsymbol{\xi}_a(t)\|^2 \\ & \times \left[\frac{2}{b}\lambda_{\min}(\Lambda) - c_{13}^2\right]\|\boldsymbol{e}_w(t)\|^2 + \frac{4c_9}{b}\|\boldsymbol{n}_r(t)\| \\ & + c_{14}\|\boldsymbol{n}_r(t)\|^2 + \frac{3}{b^2c_{12}^2}\end{aligned} \tag{94}$$

The inequality in Eq. (94) implies that $\dot{V}_3(t) \le 0$ outside the compact set:

$$\Omega_3 = \left\{\|\boldsymbol{\xi}_a\| \le \sqrt{\frac{c_{18}}{c_{15}}}, \boldsymbol{e}_w = \boldsymbol{0}, |\tilde{b}| \le \tilde{b}^*, \|\tilde{\boldsymbol{d}}\| \le \tilde{d}^*\right\} \tag{95}$$

where

$$c_{18} = c_{14}c_{17}^2 + \frac{4c_9}{b}c_{17} + \frac{3}{b^2c_{12}^2}\left(1 - a_f^{-1}\right)^2$$

Therefore, the signals $\boldsymbol{\xi}_a(t)$, $\tilde{b}(t)$, $\tilde{\boldsymbol{d}}(t)$, and $\boldsymbol{e}_w(t)$ are uniformly ultimately bounded. □

D. Gain Matrix Design

The observer gain matrix L can be chosen to minimize the mean square estimation error:

$$J_n = E\{\tilde{\boldsymbol{z}}^\top(t)\tilde{\boldsymbol{z}}(t)\} \tag{96}$$

For the linear estimate in Eq. (78) to be optimal, the estimation error must be orthogonal (in the probabilistic sense) to the measurement

data at all times (see, for example, [32], p. 233); that is,

$$E\{\tilde{z}(t)\boldsymbol{y}^{*\top}(\tau)\} = 0 \tag{97}$$

for all $\tau \leq t$. Following standard arguments ([32], p. 241), the estimation error correlation matrix $K_{\tilde{z}}(t,\tau)$ can be computed as

$$K_{\tilde{z}}(t,t)C = LK_{\boldsymbol{n}_r}(t,t) \tag{98}$$

and therefore the estimator gain matrix can be computed as

$$L = K_{\tilde{z}}(t,t)CK_{\boldsymbol{n}_r}^{-1}(t,t) \tag{99}$$

It can be verified that the evolution of the estimation error correlation matrix is described by the following differential equation (see, for example, [32], p. 71):

$$\dot{K}_{\tilde{z}}(t) = A_m K_{\tilde{z}}(t) + K_{\tilde{z}}(t)A_m^{\top} - K_{\tilde{z}}(t)C^{\top}K_{\boldsymbol{n}_r}(t)^{-1}CK_{\tilde{z}}(t) \tag{100}$$

If we assume a constant correlation matrix $K_{\boldsymbol{n}_r}$ for the measurement noise $\boldsymbol{n}_r(t)$, the steady-state estimator gain can be computed using the standard Ricatti algebraic equation:

$$0 = A_m K_{\tilde{z}} + K_{\tilde{z}}A_m^{\top} - K_{\tilde{z}}C^{\top}K_{\boldsymbol{n}_r}^{-1}CK_{\tilde{z}} \qquad L = K_{\tilde{z}}CK_{\boldsymbol{n}_r}^{-1} \tag{101}$$

In either case, one needs to make sure that the conditions $l_{i1} \geq \lambda_i$ and $l_{i2} > 0$ are satisfied. Otherwise, a suboptimal gain matrix can be chosen.

Remark 3. The nonlinear observation model in Eq. (71) can lead to a bias plus a Gaussian noise component. We approximate the nonlinear functions by the first-order Taylor series expansion, such as in the extended Kalman filter applications (see, for example, [33]). In this case, in the expression $r^*(t) = r(t) + n_r(t)$, the signal

$$n_r(t) = L_{E/B}\nabla \boldsymbol{f}(y_I(t), z_I(t), b_I(t))n_I(t)$$

is a linear function of zero-mean Gaussian noise $n_I(t)$. The neglected terms in the preceding approximation are of higher order in $n_I(t)$ and are small for small values of measurement noise. The zero-mean Gaussian assumption for $n_r(t)$ is not crucial for the stability of the system, because Theorem 3 guarantees bounded tracking errors for any bounded noise process $n_r(t)$ whether it has a bias term or not. However, the error correlation matrix $K_{\tilde{z}}$ and, hence, the filter gain matrix L_f will be affected. The investigation of this effect is not pursued in the paper.

V. Flight Control Design

A. Guidance Formulation

Because the inertial acceleration does not directly enter into aircraft dynamics, we need to first determine the corresponding states associated with the desired acceleration command $\boldsymbol{a}_F$. These states can be used later as reference inputs to define the control surface deflections for the follower aircraft to track. The inertial velocity of the aircraft is readily obtained by integrating the acceleration:

$$\boldsymbol{V}_F(t) = \boldsymbol{V}_F(0) + \int_0^t \boldsymbol{a}_F(\tau)\,\mathrm{d}\tau$$

Therefore, the airspeed

$$\mathrm{V}_c(t) = \|\boldsymbol{V}_F(t)\| \tag{102}$$

the flight path angle

$$\gamma = -\sin^{-1}\left(\frac{V_{Fx}}{\mathrm{V}_c}\right) \tag{103}$$

and the azimuth angle

$$\chi = \tan^{-1}\left(\frac{V_{Fy}}{V_{Fy}}\right) \tag{104}$$

can be computed from its components. Next, we compute the aircraft attitude angles. To this end, recall that the inertial forces acting on the aerial vehicle can be calculated from Newton's second law:

$$\boldsymbol{F} = m\boldsymbol{a}_F \tag{105}$$

where m is the aircraft's mass. The inertial force can be transformed into the wind-axis force as follows:

$$\boldsymbol{F}^W = L_{W/E}\boldsymbol{F} \tag{106}$$

where $L_{W/E}$ is the coordinate transformation matrix from the inertial frame to the wind frame, defined similar to $L_{B/E}$ in Eq. (9) by replacing the body-axis Euler angles ϕ, θ, and ψ with the wind-axis Euler angles μ, γ, and χ, where angles γ and χ are already computed, and the wind-axis roll angle μ still needs to be determined. Using the wind-axis force components [23], we can write the following equation:

$$\begin{bmatrix} T\cos\alpha\cos\beta - D - mg\sin\gamma \\ -T\cos\alpha\sin\beta - C + mg\sin\mu\cos\gamma \\ -T\sin\alpha - L + mg\cos\mu\cos\gamma \end{bmatrix} = \boldsymbol{F}^W \tag{107}$$

where T is the thrust, D is the drag, C is the side force, L is the lift, α is the angle of attack, β is the sideslip angle, and g is the gravity acceleration. In these three equations, we have seven unknowns: T, D, C, L, α, β, and μ. One more equation can be obtained from the condition that all the turns made by the aircraft are perfectly coordinated [34]; that is, the side force is zero. In this case, we can assume that the sideslip angle can be neglected. Therefore, the second equation in Eq. (107) reduces to

$$mg\sin\mu\cos\gamma = F_y^W \tag{108}$$

from which μ can be computed as follows:

$$\tan\mu = \frac{a_{Fx}\sin\chi - a_{Fy}\cos\chi}{a_{Fx}\sin\gamma\cos\chi + a_{Fy}\sin\gamma\sin\chi + (a_{Fz} - g)\cos\gamma}$$

Neglecting β in the remaining two equations in Eq. (107) leads to

$$\begin{aligned} T\cos\alpha - D - mg\sin\gamma &= F_x^W \\ -T\sin\alpha - L + mg\cos\mu\cos\gamma &= F_z^W \end{aligned} \tag{109}$$

where F_x^W and F_z^W are the wind-axis force components that are now available. Here, we recall that the control surface deflections are primarily moment generators for the conventional aircraft with no direct force control. Therefore, the dependence of the lift and drag forces on these deflections can be neglected: $C_D = C_D(\alpha)$ and $C_L = C_L(\alpha, \dot{\alpha}, q)$, where $C_D = D/\bar{q}S$ and $C_L = L/\bar{q}S$ are, respectively, the drag and lift coefficients; $\bar{q} = \frac{1}{2}\rho\mathrm{V}_c^2$ is the dynamic pressure; ρ is the air density; S is the aircraft's reference area; and q is the pitch rate. The presence of q in the lift coefficient will require differentiation of the wind axis Euler angles can be done numerically, as it is done in [35], in which case solving Eqs. (109) will result in a differential equation for α. Here, we make a simplifying assumption that the lift dependence on the angle of attack and pitch rates is negligible, so that $C_L = C_L(\alpha) = C_{LO} + C_{L\alpha}\alpha$. The drag force can be expressed using the parabolic drag polar equation $C_D = C_{D0} + kC_L$ or simply $C_D = C_{D0} + C_{D0}\alpha$. Here, we will use the latter. From Eqs. (109), we can easily derive the following equation for α:

$$\begin{aligned} -D\sin\alpha - L\cos\alpha &= \left(F_x^W + mg\sin\gamma\right)\sin\alpha \\ &+ \left(F_z^W - mg\cos\mu\cos\gamma\right)\cos\alpha \end{aligned} \tag{110}$$

With $\beta = 0$, the transformation matrix $L_{B/W}$ from the wind to body axis reduces to

$$L_{B/W} = \begin{bmatrix} \cos\alpha & 0 & -\sin\alpha \\ 0 & 1 & 0 \\ \sin\alpha & 0 & \cos\alpha \end{bmatrix} \tag{111}$$

Using the relationship $L_{B/E} = L_{B/W} L_{W/E}$, the body-axis Euler angles can be computed as follows:

$$\phi_c = \tan^{-1}\left(\frac{L_{B/E}(2,3)}{L_{B/E}(3,3)}\right), \qquad \theta_c = -\sin^{-1}(L_{B/E}(1,3))$$
$$\psi_c = \tan^{-1}\left(\frac{L_{B/E}(1,2)}{L_{B/E}(1,1)}\right) \tag{112}$$

where $L_{B/E}(i,j)$ denotes the (i,j)th entry of the matrix $L_{B/E}$.

B. Aircraft Model

Consider the dynamic equations of the aircraft written in a combined wind and body axis [34]:

$$\begin{aligned}
\dot{\mathbb{V}}(t) &= \frac{1}{m}[-D - mg\sin\gamma(t) + T\cos\beta(t)\cos\alpha(t)] \\
\dot{\alpha}(t) &= q(t) - p(t)\cos\alpha(t)\tan\beta(t) - r(t)\sin\alpha(t)\tan\beta(t) \\
&\quad - q_w(t)\sec\beta(t) \\
\dot{\beta}(t) &= r_w(t) + p(t)\sin\alpha(t) - r(t)\cos\alpha(t) \\
\begin{bmatrix}\dot{\phi}(t)\\ \dot{\theta}(t)\\ \dot{\psi}(t)\end{bmatrix} &= P(t)\begin{bmatrix}p(t)\\ q(t)\\ r(t)\end{bmatrix} \\
J\begin{bmatrix}\dot{p}(t)\\ \dot{q}(t)\\ \dot{r}(t)\end{bmatrix} &= -\begin{bmatrix}p(t)\\ q(t)\\ r(t)\end{bmatrix} \times J\begin{bmatrix}p(t)\\ q(t)\\ r(t)\end{bmatrix} + \begin{bmatrix}\mathcal{L}\\ \mathcal{M}\\ \mathcal{N}\end{bmatrix}
\end{aligned} \tag{113}$$

with

$$P(t) = \begin{bmatrix} 1 & \sin\phi(t)\tan\theta(t) & \cos\phi(t)\tan\theta(t) \\ 0 & \cos\phi(t) & -\sin\phi(t) \\ 0 & \sin\phi(t)\sec\theta(t) & \cos\phi(t)\sec\theta(t) \end{bmatrix}$$

$$r_w(t) = \frac{1}{m\mathbb{V}(t)}[-C + mg\sin\mu(t)\cos\gamma(t) - T\sin\beta(t)\cos\alpha(t)]$$

$$q_w(t) = \frac{1}{m\mathbb{V}(t)}[L - mg\cos\mu(t)\cos\gamma(t) + T\sin\alpha(t)]$$

$$J = \begin{bmatrix} J_{xx} & 0 & -J_{xz} \\ 0 & J_{yy} & 0 \\ -J_{xz} & 0 & J_{zz} \end{bmatrix} \tag{114}$$

where $\mathbb{V}$ is the airspeed, p is the roll rate, r is the yaw rate, and J is the follower's inertia matrix. The body-axis moments are expressed in the form

$$\mathcal{L} = \mathcal{L}_n + \mathcal{L}_T + \Delta_l, \qquad \mathcal{M} = \mathcal{M}_n + \mathcal{M}_T + \Delta_m$$
$$\mathcal{N} = \mathcal{N}_n + \mathcal{N}_T + \Delta_n \tag{115}$$

where $\mathcal{L}_n$, $\mathcal{M}_n$, and $\mathcal{N}_n$ are respective nominal aerodynamic moments that are known and linear in control surface deflections; $\mathcal{L}_T$, $\mathcal{M}_T$, and $\mathcal{N}_T$ are body-axis moments due to engine thrust; and Δ_l, Δ_m, and Δ_n represent uncertainties in the aerodynamic moments not accounted for in the nominal moments. They are associated with the modeling of the aircraft dynamics and the turbulent effect of the closed coupled formation flight. In general, these are unknown functions of states $\boldsymbol{\xi} = [\mathbb{V} \quad \alpha \quad \beta \quad p \quad q \quad r]^\top$ of the system in Eq. (113) and control $\boldsymbol{u} = [\delta_T \quad \delta_a \quad \delta_e \quad \delta_r]^\top$, where δ_T, δ_e, δ_a, and δ_r are, respectively, the throttle, elevator, aileron, and rudder deflections. The aerodynamic forces D, C, and L also are assumed to have nominal known parts D_n, C_n, and L_n and unknown parts $\Delta_D(\boldsymbol{\xi},\boldsymbol{u})$, $\Delta_C(\boldsymbol{\xi},\boldsymbol{u})$, and $\Delta_L(\boldsymbol{\xi},\boldsymbol{u})$. The control algorithm presented later will compensate for the uncertainties in the aerodynamic drag force and aerodynamic moments that are assumed to be bounded and continuous functions of $\boldsymbol{\xi}$, $\boldsymbol{u} \in \mathcal{D}$, where $\mathcal{D}$ is a compact set of corresponding possible initial conditions. For these unknown functions, we will use linear in parameter approximations by neural networks with RBFs in its hidden layer [36]:

$$\begin{aligned}
\frac{1}{m}\Delta_D(\boldsymbol{\xi},\boldsymbol{u}) &= \boldsymbol{W}_D^\top \boldsymbol{\Phi}(\boldsymbol{\xi},\boldsymbol{u}) + \epsilon_D(\boldsymbol{\xi},\boldsymbol{u}) \\
J^{-1}\begin{bmatrix}\Delta_l(\boldsymbol{\xi},\boldsymbol{u})\\ \Delta_m(\boldsymbol{\xi},\boldsymbol{u})\\ \Delta_n(\boldsymbol{\xi},\boldsymbol{u})\end{bmatrix} &= \begin{bmatrix}\boldsymbol{W}_l^\top \boldsymbol{\Phi}(\boldsymbol{\xi},\boldsymbol{u}) + \epsilon_l(\boldsymbol{\xi},\boldsymbol{u})\\ \boldsymbol{W}_m^\top \boldsymbol{\Phi}(\boldsymbol{\xi},\boldsymbol{u}) + \epsilon_n(\boldsymbol{\xi},\boldsymbol{u})\\ \boldsymbol{W}_n^\top \boldsymbol{\Phi}(\boldsymbol{\xi},\boldsymbol{u}) + \epsilon_n(\boldsymbol{\xi},\boldsymbol{u})\end{bmatrix} \\
\|\epsilon_D(\boldsymbol{\xi},\boldsymbol{u})\| &\le \epsilon_D^*, \qquad \|\epsilon_l(\boldsymbol{\xi},\boldsymbol{u})\| \le \epsilon_l^* \\
\|\epsilon_m(\boldsymbol{\xi},\boldsymbol{u})\| &\le \epsilon_m^*, \qquad \|\epsilon_n(\boldsymbol{\xi},\boldsymbol{u})\| \le \epsilon_n^*
\end{aligned} \tag{116}$$

where $\boldsymbol{w}_i \in \mathbb{R}^{N_i}$ $(i = D, l, m, n)$ are the vectors of unknown constant parameters and $\boldsymbol{\Phi}(\boldsymbol{\xi},\boldsymbol{u})$ is the vector of RBFs. We further assume that the thrust and nominal aerodynamic moments can be represented as follows:

$$\begin{aligned}
T &= \tfrac{1}{2}\rho\mathbb{V}^2 S C_{T_{\delta_T}}\delta_T \\
\mathcal{L}_n &= \tfrac{1}{2}\rho\mathbb{V}^2 Sb[C_l(\beta,p,r) + C_{l_{\delta_a}}\delta_a + C_{l_{\delta_r}}\delta_r] \\
\mathcal{N}_n &= \tfrac{1}{2}\rho\mathbb{V}^2 Sb[C_n(\beta,p,r) + C_{n_{\delta_a}}\delta_a + C_{n_{\delta_r}}\delta_r] \\
\mathcal{M}_n &= \tfrac{1}{2}\rho\mathbb{V}^2 S\bar{c}[C_m(M,\alpha,q) + C_{m_{\delta_e}}\delta_e]
\end{aligned} \tag{117}$$

where ρ is the air density. Here, b_F is the follower's wing span; $\bar{c}$ is the mean-aerodynamic chord; $C_{T_{\delta T}}$, $C_{l_{\delta_a}}$, $C_{l_{\delta_r}}$, $C_{n_{\delta_a}}$, $C_{n_{\delta_r}}$, and $C_{m_{\delta_e}}$ are the corresponding control effectiveness; and C_l, C_n, and C_m are the aerodynamic coefficients.

C. Control Surface Deflections Design

In this subsection, we derive the control surface deflection commands $\boldsymbol{u} = [\delta_T \quad \delta_e \quad \delta_a \quad \delta_r]^\top$ to track the desired motion. Because there are four control inputs, we chose $\mathbb{V}$, ϕ, θ, and ψ as the regulated outputs to track the desired velocity and attitude commands $\mathbb{V}_c$, ϕ_c, θ_c, and ψ_c in Eqs. (102) and (112). For this purpose, we first derive desired laws for X_T, $\mathcal{L}_n$, $\mathcal{M}_n$, and $\mathcal{N}_n$ for the dynamics in Eq. (113) to track the reference commands $[\mathbb{V}_c(t), \phi_c(t), \theta_c(t), \psi_c(t)]$. These can be inverted afterward to obtain the actual throttle and control surface deflections using the relationships in Eq. (117).

1. *Velocity Control*

We start with the first equation in Eq. (113) to design the tracking control law for the velocity command $\mathbb{V}_c(t)$ and set

$$\begin{aligned}
T(t) = \frac{1}{\cos\alpha(t)\cos\beta(t)}\{&mg\sin\gamma(t) + D^n(\boldsymbol{\xi}(t),\boldsymbol{u}(t)) \\
&+ m\hat{\boldsymbol{W}}_D^\top(t)\boldsymbol{\Phi}(\boldsymbol{\xi}(t),\boldsymbol{u}(t)) - mk_{\mathbb{V}}(\mathbb{V}(t) - \mathbb{V}_c(t)) + m\dot{\mathbb{V}}_c(t)\}
\end{aligned} \tag{118}$$

where $k_{\mathbb{V}} > 0$ is the desired time constant (design parameter), and $\hat{\boldsymbol{W}}_D(t)$ is the estimate of the unknown weight vector $\boldsymbol{W}_D$, which is updated online. Defining the tracking error as $e_{\mathbb{V}} = \mathbb{V}(t) - \mathbb{V}_c(t)$, the error dynamics can be written as

$$\dot{e}_{\mathbb{V}}(t) = -k_{\mathbb{V}} e_{\mathbb{V}}(t) - \tilde{\boldsymbol{W}}_D^\top(t)\boldsymbol{\Phi}(\boldsymbol{\xi}(t),\boldsymbol{u}(t)) - \epsilon_D(\boldsymbol{\xi}(t),\boldsymbol{u}(t)) \tag{119}$$

where $\tilde{\boldsymbol{W}}_D(t) = \hat{\boldsymbol{W}}_D(t) - \boldsymbol{W}_D$ is the parameter error. The adaptive law for the estimate $\hat{\boldsymbol{W}}_D(t)$ is designed using the following Lyapunov function candidate:

$$V_4(e_{\mathbb{V}}(t), \tilde{\boldsymbol{W}}_D(t)) = \tfrac{1}{2}e_{\mathbb{V}}^2(t) + \tilde{\boldsymbol{W}}_D^\top(t) G_D^{-1} \tilde{\boldsymbol{W}}_D(t) \tag{120}$$

where $G_D > 0$ is the adaptive gain. It is straightforward to verify that the derivative of $V_4(t)$ along the trajectory of the system in Eq. (119) satisfies the inequality

$$\dot{V}_4(e_{\mathbb{V}}(t), \tilde{\boldsymbol{W}}_D(t)) \le -k_{\mathbb{V}} e_{\mathbb{V}}^2(t) - e_{\mathbb{V}}(t)\epsilon_D(\boldsymbol{\xi}(t),\boldsymbol{u}(t)) \tag{121}$$

if we set

$$\dot{\hat{\boldsymbol{W}}}_D(t) = G_D \text{Proj}(\hat{\boldsymbol{W}}_D(t), e_{\mathrm{V}}(t)\boldsymbol{\Phi}(\boldsymbol{\xi}(t), \boldsymbol{u}(t))) \tag{122}$$

where $\text{Proj}(\cdot,\cdot)$ is the projection operator and guarantees boundedness of the estimate $\hat{\boldsymbol{W}}_D(t)$ and, thus, boundedness of the parameter error $\tilde{\boldsymbol{W}}_D(t)$. Therefore, the inequality in Eq. (121) implies that the tracking error is uniformly ultimately bounded.

2. Orientation Control

Next we use the block-backstepping technique from [20] to design the pseudocontrols $p_c(t)$, $q_c(t)$, and $r_c(t)$ for the Euler angles dynamic equations to track the reference commands $\phi_c(t)$, $\theta_c(t)$, and $\psi_c(t)$. To this end, we set

$$\begin{bmatrix} p_c(t) \\ q_c(t) \\ r_c(t) \end{bmatrix} = H(t) \begin{bmatrix} -k_\phi[\phi(t) - \phi_c(t)] + \dot{\phi}_c(t) \\ -k_\theta[\theta(t) - \theta_c(t)] + \dot{w}_c(t) \\ -k_\psi[\psi(t) - \psi_c(t)] + \dot{\psi}_c(t) \end{bmatrix}$$

where $k_\phi > 0$, $k_\theta > 0$, and k_ψ are the desired time constants (design parameters), and

$$H(t) = \begin{bmatrix} 1 & 0 & -\sin\theta(t) \\ 0 & \cos\phi(t) & \sin\phi(t)\cos\theta(t) \\ 0 & -\sin\phi(t) & \cos\phi(t)\cos\theta(t) \end{bmatrix}$$

Then defining the tracking errors as

$$e_\phi(t) = \phi(t) - \phi_c(t), \qquad e_\theta(t) = \theta(t) - \theta_c(t)$$
$$e_\psi(t) = \psi(t) - \psi_c(t)$$

the corresponding error dynamics result in the system

$$\dot{e}_\phi(t) = -k_\phi e_\phi(t), \qquad \dot{e}_\theta(t) = -k_\theta e_\theta(t), \qquad \dot{e}_\psi(t) = -k_\psi e_\psi(t) \tag{123}$$

which are exponentially stable. Therefore, denoting the corresponding errors by

$$e_p(t) = p(t) - p_c(t), \qquad e_q(t) = q(t) - q_c(t)$$
$$e_r(t) = r(t) - r_c(t)$$

and designing the nominal aerodynamic moments as

$$\begin{bmatrix} \mathcal{L}_n(t) \\ \mathcal{M}_n(t) \\ \mathcal{N}_n(t) \end{bmatrix} = \begin{bmatrix} p(t) \\ q(t) \\ r(t) \end{bmatrix} \times J \begin{bmatrix} p(t) \\ q(t) \\ r(t) \end{bmatrix} - JP(t) \begin{bmatrix} e_\phi(t) \\ e_\theta(t) \\ e_\psi(t) \end{bmatrix}$$
$$- J \begin{bmatrix} \hat{\boldsymbol{W}}_l^\top(t)\boldsymbol{\Phi}(\boldsymbol{\xi}, \boldsymbol{u}) \\ \hat{\boldsymbol{W}}_m^\top(t)\boldsymbol{\Phi}(\boldsymbol{\xi}, \boldsymbol{u}) \\ \hat{\boldsymbol{W}}_n^\top(t)\boldsymbol{\Phi}(\boldsymbol{\xi}, \boldsymbol{u}) \end{bmatrix} + J \begin{bmatrix} -k_p e_p(t) + \dot{p}_c(t) \\ -k_q e_q(t) + \dot{q}_c(t) \\ -k_r e_r(t) + \dot{r}_c(t) \end{bmatrix} \tag{124}$$

where $k_p > 0$, $k_r > 0$, $k_q > 0$ are the desired time constants (design parameters) and $\hat{\boldsymbol{W}}_l(t)$, $\hat{\boldsymbol{W}}_m(t)$, and $\hat{\boldsymbol{W}}_n(t)$ are, respectively, the estimates of the unknown weight vectors $\boldsymbol{W}_l$, $\boldsymbol{W}_m$, and $\boldsymbol{W}_n$ that are updated online. The overall error dynamics can be written as follows:

$$\begin{bmatrix} \dot{e}_\phi(t) \\ \dot{e}_\theta(t) \\ \dot{e}_\psi(t) \end{bmatrix} = \begin{bmatrix} -k_\phi e_\phi(t) \\ -k_\theta e_\theta(t) \\ -k_\psi e_\psi(t) \end{bmatrix} + P(t) \begin{bmatrix} e_p(t) \\ e_q(t) \\ e_r(t) \end{bmatrix}$$
$$\begin{bmatrix} \dot{e}_p(t) \\ \dot{e}_q(t) \\ \dot{e}_r(t) \end{bmatrix} = \begin{bmatrix} -k_p e_p(t) \\ -k_q e_q(t) \\ -k_r e_r(t) \end{bmatrix} - P(t) \begin{bmatrix} e_\phi(t) \\ e_\theta(t) \\ e_\psi(t) \end{bmatrix}$$
$$- \begin{bmatrix} \tilde{\boldsymbol{W}}_l^\top(t)\boldsymbol{\Phi}(\boldsymbol{\xi}(t), \boldsymbol{u}(t)) - \epsilon_l(\boldsymbol{\xi}(t), \boldsymbol{u}(t)) \\ \tilde{\boldsymbol{W}}_m^\top(t)\boldsymbol{\Phi}(\boldsymbol{\xi}(t), \boldsymbol{u}(t)) - \epsilon_m(\boldsymbol{\xi}(t), \boldsymbol{u}(t)) \\ \tilde{\boldsymbol{W}}_n^\top(t)\boldsymbol{\Phi}(\boldsymbol{\xi}(t), \boldsymbol{u}(t)) - \epsilon_n(\boldsymbol{\xi}(t), \boldsymbol{u}(t)) \end{bmatrix} \tag{125}$$

where

$$\tilde{\boldsymbol{W}}_l(t) = \hat{\boldsymbol{W}}_l(t) - \boldsymbol{W}_l, \qquad \tilde{\boldsymbol{W}}_m(t) = \hat{\boldsymbol{W}}_m(t) - \boldsymbol{W}_m$$
$$\tilde{\boldsymbol{W}}_n(t) = \hat{\boldsymbol{W}}_n(t) - \boldsymbol{W}_n$$

are the parameter estimation errors.

Consider the following Lyapunov function candidate for the error dynamics in Eq. (125):

$$V_5(e_\phi(t), e_\theta(t), e_\psi(t), e_p(t), e_q(t), e_r(t), \tilde{\boldsymbol{W}}_l(t), \tilde{\boldsymbol{W}}_m(t), \tilde{\boldsymbol{W}}_n(t))$$
$$= +\tfrac{1}{2}e_\phi^2(t) + \tfrac{1}{2}e_\theta^2(t) + \tfrac{1}{2}e_\psi^2(t) + \tfrac{1}{2}e_p^2(t) + \tfrac{1}{2}e_q^2(t) + \tfrac{1}{2}e_r^2(t)$$
$$+ \tilde{\boldsymbol{W}}_l^\top(t)G_p^{-1}\tilde{\boldsymbol{W}}_l(t) + \tilde{\boldsymbol{W}}_m^\top(t)G_q^{-1}\tilde{\boldsymbol{W}}_m(t) + \tilde{\boldsymbol{W}}_n^\top(t)G_r^{-1}\tilde{\boldsymbol{W}}_n(t) \tag{126}$$

where $G_l > 0$, $G_m > 0$, and $G_n > 0$ are the adaptive gains. If we define the adaptive laws for the estimates $\hat{\boldsymbol{W}}_l(t)$, $\hat{\boldsymbol{W}}_m(t)$, and $\hat{\boldsymbol{W}}_n(t)$ as

$$\dot{\hat{\boldsymbol{W}}}_l(t) = G_p \text{Proj}(\hat{\boldsymbol{W}}_l(t), e_p(t)\boldsymbol{\Phi}(\boldsymbol{\xi}(t), \boldsymbol{u}(t)))$$
$$\dot{\hat{\boldsymbol{W}}}_m(t) = G_q \text{Proj}(\hat{\boldsymbol{W}}_m(t), e_q(t)\boldsymbol{\Phi}(\boldsymbol{\xi}(t), \boldsymbol{u}(t))) \tag{127}$$
$$\dot{\hat{\boldsymbol{W}}}_n(t) = G_r \text{Proj}(\hat{\boldsymbol{W}}_n(t), e_r(t)\boldsymbol{\Phi}(\boldsymbol{\xi}(t), \boldsymbol{u}(t)))$$

it can be verified that

$$\dot{V}_5(t) \le -k_\phi e_\phi^2(t) - k_\theta e_\theta^2(t) - k_\psi e_\psi^2(t) - k_p e_p^2(t)$$
$$- e_p(t)\epsilon_l(\boldsymbol{\xi}(t), \boldsymbol{u}(t)) - k_q e_q^2(t) - e_q(t)\epsilon_m(\boldsymbol{\xi}(t), \boldsymbol{u}(t))$$
$$- k_r e_r^2(t) - e_r(t)\epsilon_n(\boldsymbol{\xi}(t), \boldsymbol{u}(t)) \tag{128}$$

Taking into account the uniform bounds on the function approximation errors in Eq. (116), the following upper bound can be written:

$$\dot{V}_5(t) \le -k_\phi e_\phi^2(t) - k_\theta e_\theta^2(t) - k_\psi e_\psi^2(t) - |e_p(t)|[k_p|e_p(t)| - \epsilon_l^*]$$
$$- |e_q(t)|[k_q|e_q(t)| - \epsilon_m^*] - |e_r(t)|[k_r|e_r(t)| - \epsilon_n^*] \tag{129}$$

It follows that $\dot{V}_5(t) \le 0$ outside the compact region:

$$\Omega = \{|e_p(t)| \le k_p^{-1}\epsilon_l^*, |e_q(t)| \le k_q^{-1}\epsilon_m^*, |e_r(t)|$$
$$\le k_r^{-1}\epsilon_n^*, \|\tilde{\boldsymbol{W}}_i(t)\| \le W_i^*, \ i = l, m, n\} \tag{130}$$

where the bounds W_i^* are guaranteed by the projection operator used in the adaptive laws in Eq. (127), implying ultimate boundedness of all error signals.

The throttle and control surface deflections are easily found by solving Eqs. (118) and (124) for δ_T, δ_a, δ_e, and δ_r, because the nominal aerodynamic moments are assumed to have linear representations in control surface deflections. The derivation of the control laws is summarized in the following theorem:

Theorem 4. The aircraft thrust and the aerodynamic moments defined in Eqs. (118) and (124), along with the adaptive laws in Eqs. (122) and (127), guarantee tracking of the reference commands $\mathrm{V}_c(t)$, $\phi_c(t)$, $\theta_c(t)$, and $\psi_c(t)$ with uniformly ultimately bounded errors.

If the approximation errors are zero, that is, $\epsilon_i(x) = 0$ $(i = D, l, m, n)$, then it follows from Eqs. (121) and (129) that for all $\boldsymbol{\xi}$, $\dot{V}_4(t) \le 0$ and $\dot{V}_5(t) \le 0$. Using Barbalat's Lemma, one can show asymptotic tracking of the acceleration command $\boldsymbol{a}_F$.

Remark 4. The control laws in Eqs. (118) and (124) contain the derivatives of the reference commands $\mathrm{V}_c(t)$, $\phi_c(t)$, $\theta_c(t)$, and $\psi_c(t)$ that involve unknown disturbances $\boldsymbol{a}_T(t)$ through the guidance law in Eq. (51). To overcome the situation, one can prefilter the reference commands $\mathrm{V}_c(t)$, $\phi_c(t)$, $\theta_c(t)$, and $\psi_c(t)$ by a stable low-pass filter. For instance, for the $\mathrm{V}(t)$ dynamics, one can set

$$\dot{\mathrm{V}}_m(t) = -\lambda_{\mathrm{V}}[\mathrm{V}_m(t) - \mathrm{V}_c(t)] \tag{131}$$

where $\lambda_{\mathrm{V}} > 0$ is a constant. In the control law in Eq. (118), one can use $\mathrm{V}_m(t)$ instead of $\mathrm{V}_c(t)$ and replace the derivative $\dot{\mathrm{V}}_m(t)$ with the

right-hand side of Eq. (131). To remove the steady-state error, one can define the integral error

$$\mathbb{V}_I(t) = \int_{t_0}^{t} [\mathbb{V}_m(\tau) - \mathbb{V}_c(\tau)]\,\mathrm{d}\tau$$

and write the extended dynamics:

$$\begin{aligned} \dot{\mathbb{V}}_I(t) &= \mathbb{V}_m(t) - \mathbb{V}_c(t) \\ \dot{\mathbb{V}}_m(t) &= -2\zeta_u\omega_{\mathbb{V}}[\mathbb{V}_m(t) - \mathbb{V}_c(t)] - \omega_{\mathbb{V}}^2\mathbb{V}_I(t) \end{aligned} \tag{132}$$

where $\zeta_{\mathbb{V}}$ and $\omega_{\mathbb{V}}$ are the desired damping ratio and frequency (design parameters). Again, the command $\mathbb{V}_c(t)$ can be replaced with $\mathbb{V}_m(t)$ in the control law in Eq. (118), its derivative being calculated according to the dynamics in Eq. (132).

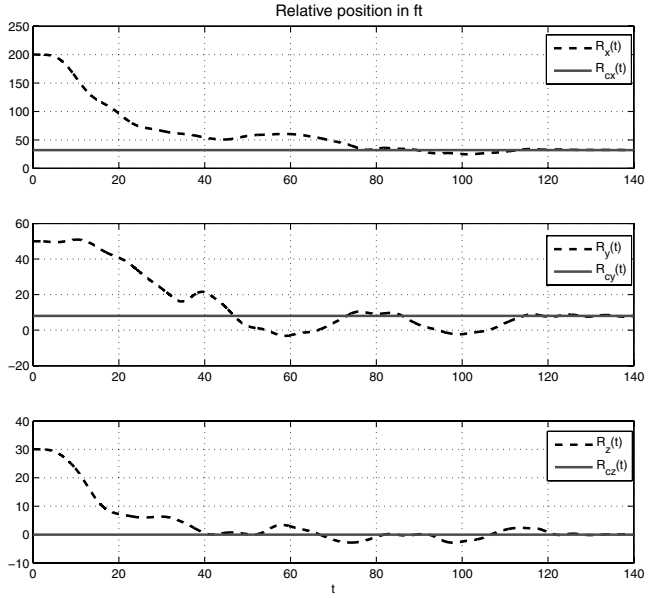

Fig. 2 Target's and follower's relative position.

VI. Simulations

The proposed algorithm is simulated for small UAV models with the following parameters: $m = 0.6293$ slugs, $J = [0.1230\ \ 0\ \ 0;\ \ 0\ \ 0.1747\ \ 0;\ \ 0\ \ 0\ \ 0.2553]$ slugs $\cdot$ ft^2, $S = 11.5$ ft^2, $c = 1.2547$ ft, and $b_F = 9.1$ ft. For the target model, a UAV is chosen with a wing span (maximal size) of 8 ft. The target makes turning, climbing, diving, and linearly accelerating maneuvers with the speed range from 35 to 60 ft/s and acceleration up to 5 ft/s^2. In simulations, an ideal pinhole camera model is used. The tracking error for feedback is formed according to

$$\boldsymbol{e}_c(t) = \boldsymbol{r}(t) - \boldsymbol{y}_m(t) + \boldsymbol{n}(t) \tag{133}$$

where $\boldsymbol{n}(t)$ is Gaussian white noise with the signal-to-noise ratio (SNR) 25 representing the effects of the actual visual sensor. The target starts its motion from the straight level flight with the airspeed $\boldsymbol{V}_{T_0} = [50\ \ 0\ \ 0]^\top$ ft/s from the position $\boldsymbol{R}_{T_0} = [200\ \ 50\ \ 30]^\top$, for which the origin of the inertial frame is placed in the follower's initial position. The follower is initially in straight level flight with the same speed and is commanded to maintain the relative coordinates $\boldsymbol{R}_c = [32\ \ 8\ \ 0]^\top$ ft. The initial conditions for the reference model and observer are set identical and equal to

$$z_m(0) = \hat{z}_m(0) = (1/\hat{b}_0)[200\ \ 0\ \ 50\ \ 0\ \ 30\ \ 0]^\top$$

where we set $\hat{b}_0 = 4$ ft. The excitation signal is added to the R_{cy} coordinate, with the amplitude defined according to Eq. (39), where $T = 2\pi/\omega$ is the period of the excitation signal $a\sin(\omega t)$, $k_i > 0$ $(i = 1, 2, 3)$ are design constants set to $T = 3$ s, $k_1 = 0.4$, $k_2 = 50$, and k_3 is set to zero. Such selection of k_3 is justified by the presence of noise. The matrix Λ for the filter in Eq. (14) is chosen as $\Lambda = \mathrm{diag}(2, 2, 2)$. The reference model is chosen with the matrices $A_m = A - \bar{B}K$, where $K = \mathrm{diag}(\mathcal{K}_1, \mathcal{K}_2, \mathcal{K}_3)$, with $\mathcal{K}_i = [1.75\ \ 0.5]$ $(i = 1, 2, 3)$, and $B_m = \bar{B}KC^\top = \mathrm{diag}(\mathcal{B}_{m1}, \mathcal{B}_{m2}, \mathcal{B}_{m3})$, where $\mathcal{B}_{mi} = [1.75\ \ 3.45]^\top$ $(i = 1, 2, 3)$. So the reference model has the poles at $-1.3625 \pm 1.2624j$ and its transfer matrix

$$G(s) = 1.75\frac{s+2}{s^2 + 2.75s + 3.5}\mathbb{I}_{3\times 3}$$

is SPR. The observer is designed with the gain matrix

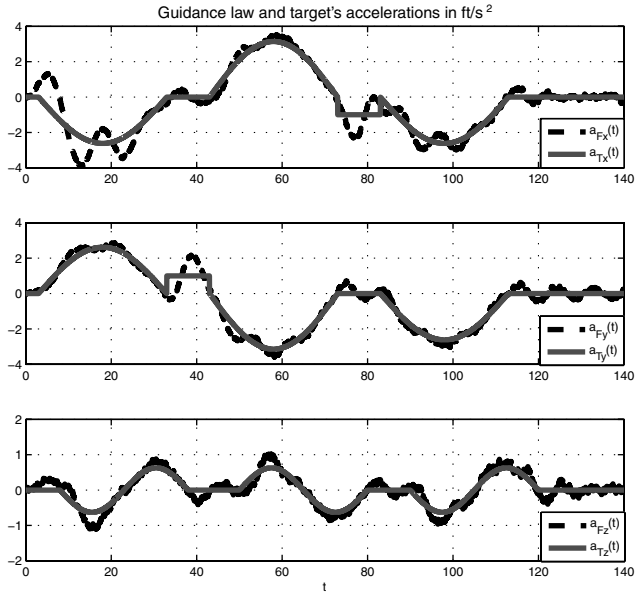

a) Accelaration command from the guidance law vs target's inertial accelerations

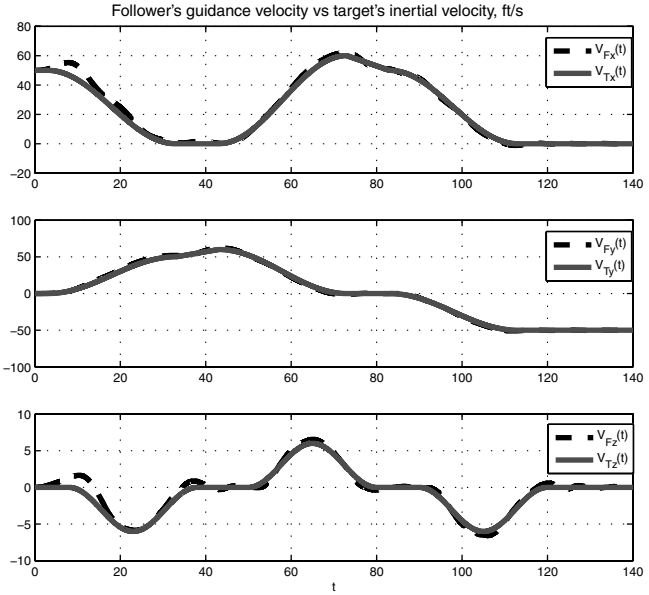

b) Target's and follower's inertial velocities

Fig. 3 Inertial velocities and accelerations.

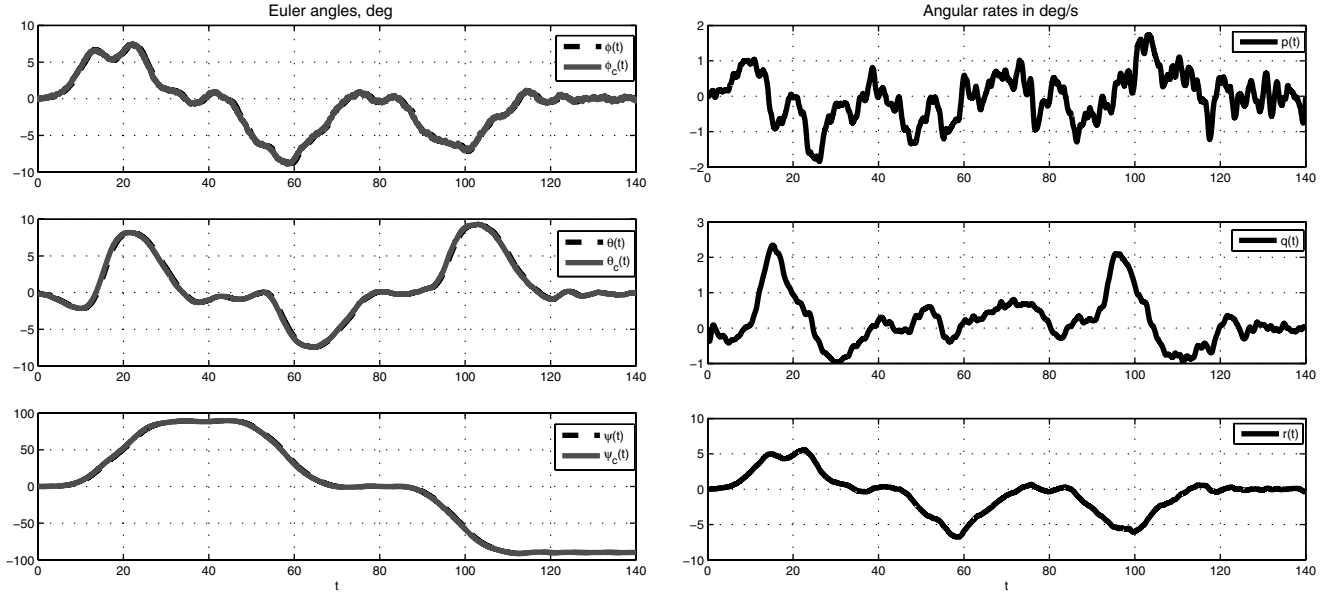

a) Euler angle responses **b) Angular rate responses**

Fig. 4 UAV responses to the guidance command.

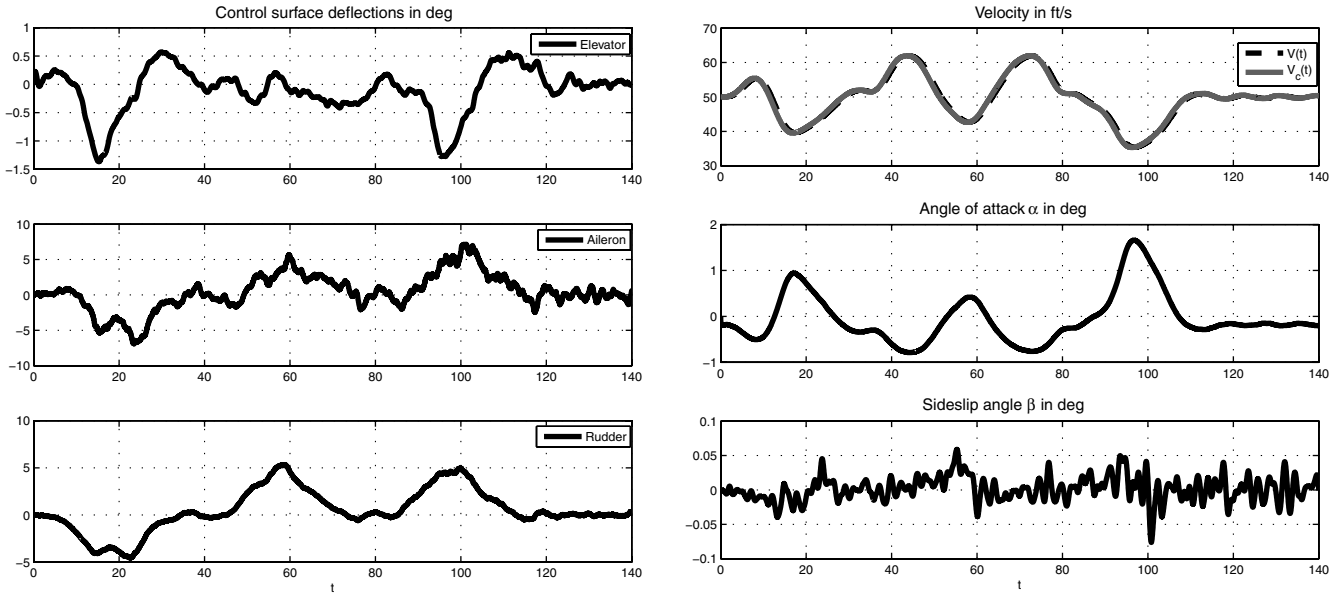

a) Control surface deflections **b) Airspeed, angle of attack and sideslip**

Fig. 5 Flight control performance.

$$L = \begin{bmatrix} 2 & 1.6 & 0 & 0 & 0 & 0 \\ 0 & 0 & 2 & 1.6 & 0 & 0 \\ 0 & 0 & 0 & 0 & 2 & 1.6 \end{bmatrix}^{\top}$$

which makes $A - LC$ Hurwitz and satisfies the SPR condition. The approximation of the signum function is done according to the relationships in Eq. (43) with $\chi = 0.5$. The guidance law is implemented according to Eqs. (79) and (81). To maintain the realistic control bounds during the transient, the following saturations are imposed on the control surface deflections: 30 deg for the elevator, 30 deg for the aileron, and 20 deg for the rudder. However, with the target maneuvers considered in this simulation scenario, the control efforts do not exceed these bounds.

The output tracking is displayed in Fig. 2. Figure 3a shows that the guidance law closely follows the target's acceleration profile. The corresponding inertial velocities are displayed in Fig. 3b. The UAV Euler angles and angular rate responses to the commands are presented in Figs. 4a and 4b. The resulting deflection commands are displayed in Fig. 5a. The angles of attack and sideslip are within acceptable range, although they are not controlled directly (Fig. 5b).

VII. Conclusions

An adaptive control framework that rejects bounded but otherwise unknown disturbances is proposed to solve the tracking problem of a maneuvering target using only visual measurement from a monocular camera fixed on the aerial vehicle. Although no direct measurement of the relative range is available, it is shown that the coordinates of the image centroid and the image maximum size obtained through an image-processing algorithm enable the follower to maintain the desired relative position with respect to the target, provided that the reference command has an additive intelligent excitation signal. It is shown that the latter is not required for the

target interception problem. The derived acceleration law is implemented using block backstepping. The proposed algorithm is simulated for small UAVs.

Acknowledgments

This material is based upon work supported by the U.S. Air Force under contract no. FA9550-05-1-0157 and Multidisciplinary University Research Initiative (MURI) subcontract no. F49620-03-1-0401.

References

[1] Stepanyan, V., and Hovakimyan, N., "Adaptive Disturbance Rejection Controller for Visual Tracking of a Maneuvering Target," *Journal of Guidance, Control, and Dynamics*, Vol. 30, No. 4, 2007, pp. 1090–1106.
doi:10.2514/1.25034

[2] Aidala, V. J., and Hammel, S. E., "Utilization of Modified Polar Coordinates for Bearings-Only Tracking," *IEEE Transactions on Automatic Control*, Vol. 28, No. 3, 1983, pp. 283–294.
doi:10.1109/TAC.1983.1103230

[3] Levine, J., and Marino, R., "Constant-Speed Target Tracking Via Bearings-Only Measurements," *IEEE Transactions on Automatic Control*, Vol. 28, No. 1, Jan. 1992, pp. 174–182.

[4] Betser, A., Vela, P., and Tannenbaum, A., "Automatic Tracking of Flying Vehicles Using Geodesic Snakes and Kalman Filtering," *Proceedings of the 43rd IEEE Conference on Decision and Control*, Vol. 2, Inst. of Electrical and Electronics Engineers, Piscataway, NJ, 12–14 Dec. 2004, pp. 1649–1654.

[5] Cao, C., and Hovakimyan, N., "Vision-Based Air-to-Air Tracking Using Intelligent Excitation," *Proceedings of the American Control Conference*, Vol. 7, Inst. of Electrical and Electronics Engineers, Piscataway, NJ, 8–10 June 2005, pp. 5091–5096.

[6] Hepner, S. A. R., and Geering, H. P., "Adaptive Two Time-Scale Tracking Filter for Target Acceleration Estimation," *Journal of Guidance, Control, and Dynamics*, Vol. 14, No. 3, May–June 1991, pp. 581–588.

[7] Chang, W. T., and Lin, S. A., "Incremental Maneuver Estimation Model for Target Tracking," *IEEE Transactions on Aerospace and Electronic Systems*, Vol. 28, No. 2, Apr. 1992, pp. 439–451.
doi:10.1109/7.144570

[8] Oshman, Y., and Shinar, J., "Using a Multiple Model Adaptive Estimator in a Random Evasion Missile/Aircraft Estimation," AIAA Guidance, Navigation and Control Conference, AIAA Paper 99-4141, 1999.

[9] Bar-Shalom, Y., and Li, X. R., *Estimation and Tracking: Principles, Techniques and Software*, Artech House, Boston, 1993.

[10] Gurfil, P., and Kasdin, N. J., "Optimal Passive and Active Tracking Using the Two-Step Estimator," AIAA Guidance, Navigation and Control Conference, AIAA Paper 2002-5022, 2002.

[11] Gurfil, P., Jodorkovsky, M., and Guelman, M., "Neoclassical Guidance for Homing Missiles," *Journal of Guidance, Control, and Dynamics*, Vol. 24, No. 3, 2001, pp. 452–459.

[12] Balakrishnan, S. N., "Extension of Modified Polar Coordinates and Application with Passive Measurements," *Journal of Guidance, Control, and Dynamics*, Vol. 12, No. 6, 1989, pp. 906–912.

[13] Stallard, D. V., "Angle-Only Tracking Filter in Modified Spherical Coordinates," *Journal of Guidance, Control, and Dynamics*, Vol. 14, No. 3, 1991, pp. 694–696.

[14] Weiss, H., and Moore, J. B., "Improved Extended Kalman Filter Design for Passive Tracking," *IEEE Transactions on Automatic Control*, Vol. AC-25, No. 4, 1980, pp. 807–811.
doi:10.1109/TAC.1980.1102436

[15] Ljung, L., "Asymptotic Behavior of the Extended Kalman Filter as a Parameter Estimator for Linear Systems," *IEEE Transactions on Automatic Control*, Vol. 24, No. 1, 1979, pp. 36–50.
doi:10.1109/TAC.1979.1101943

[16] Watanabe, Y., Johnson, E. N., and Calise, A. J., "Optimal 3-D Guidance from a 2-D Vision Sensor," AIAA Guidance, Navigation, and Control Conference, Providence, RI, AIAA Paper 2004-4779, 16–19 Aug. 2004.

[17] Sattigeri, R., Calise, A. J., and Evers, J., "An Adaptive Vision-Based Approach to Decentralized Formation Control," AIAA Guidance, Navigation, and Control Conference, Providence, RI, AIAA Paper 2004-5252, 16–19 Aug. 2004.

[18] Marino, R., and Tomei, P., *Nonlinear Control Design: Geometric, Adaptive, & Robust*, Prentice–Hall, Upper Saddle River, NJ, 1995.

[19] Stepanyan, V., and Hovakimyan, N., "Robust Adaptive Observer Design for Uncertain Systems with Bounded Disturbances," *Proceedings of the IEEE Conference on Decision and Control*, Inst. of Electrical and Electronics Engineers, Piscataway, NJ, 12–15 Dec. 2005, pp. 7750–7755.

[20] Krstic, M., Kanellakopoulos, I., and Kokotovic, P., *Nonlinear and Adaptive Control Design*, Wiley, New York, 1995.

[21] Polycarpou, M. M., "Stable Adaptive Neural Control Scheme for Nonlinear Systems," *IEEE Transactions on Automatic Control*, Vol. 41, No. 3, 1996, pp. 447–451.
doi:10.1109/9.486648

[22] Lavretsky, E., and Hovakimyan, N., "Stable Adaptation in the Presence of Actuator Constraints with Flight Control Applications," *Journal of Guidance, Control, and Dynamics*, Vol. 30, No. 2, 2007, pp. 337–345.
doi:10.2514/1.26984

[23] Etkin, B., and Reid, L. D., *Dynamics of Flight: Stability and Control*, Wiley, New York, 1996.

[24] Rusnak, I., and Meir, L., "Optimal Guidance for High Order and Acceleration Constrained Missile," *Journal of Guidance, Control, and Dynamics*, Vol. 14, No. 3, 1991, pp. 589–596.

[25] Zarchan, P., "Proportional Navigation and Weaving Targets," *Journal of Guidance, Control, and Dynamics*, Vol. 18, No. 5, 1995, pp. 969–974.

[26] Weiss, H., and Hexner, G., "Modern Guidance Laws with Model Mismatch," *Proceedings of the IFAC Symposium on Missile Guidance*, Elsevier, Oxford, 1998, pp. 10–21.

[27] Gurfil, P., Jodorkovsky, M., and Guelman, M., "Design of Nonsaturating Guidance Systems," *Journal of Guidance, Control, and Dynamics*, Vol. 23, No. 4, 2001, pp. 693–700.

[28] Sastry, S. S., and Bodson, M., *Adaptive Control: Stability, Convergence and Robustness*, Prentice–Hall, Upper Saddle River, NJ, 1989.

[29] Polycarpou, M. M., and Ioannou, P. A., "On the Existence and Uniqueness of Solutions in Adaptive Control Systems," *IEEE Transactions on Automatic Control*, Vol. 38, No. 3, 1993, pp. 474–479.
doi:10.1109/9.210149

[30] Pomet, J. B., and Praly, L., "Adaptive Nonlinear Regulation: Estimation from the Lyapunov Equation," *IEEE Transactions on Automatic Control*, Vol. 37, No. 6, 1992, pp. 729–740.
doi:10.1109/9.256328

[31] Shevitz, D., and Paden, B., "Lyapunov Stability Theory of Nonsmooth Systems," *IEEE Transactions on Automatic Control*, Vol. 39, No. 9, 1994, pp. 1910–1914.
doi:10.1109/9.317122

[32] Burl, J. B., *Linear Optimal Control: $\mathcal{H}_2$ and $\mathcal{H}_\infty$ Methods*, Addison Wesley Longman, Reading, MA, 1999.

[33] Bar-Shalom, Y., and Fortmann, T., *Tracking and Data Association*, Academic Press, London, 1988.

[34] Stevens, B. L., and Lewis, F. L., *Aircraft Control and Simulation*, Wiley, New York, 1992.

[35] Munro, B., "Airplane Trajectory Expansion for Dynamics Inversion," M.S. Thesis, Aerospace and Ocean Engineering Dept., Virginia Polytechnic Inst. and State Univ., Blacksburg, VA, 1992.

[36] Park, J., and Sandberg, I., "Universal Approximation Using Radial Basis Function Networks," *Neural Computations*, Vol. 3, No. 2, 1991, pp. 246–257.